Comparison of network-based models for rubber

Antoine Gloria, Patrick Le Tallec, Marina Vidrascu

COMPARISON OF NETWORK-BASED MODELS FOR RUBBER

ANTOINE GLORIA, PATRICK LE TALLEC, AND MARINA VIDRASCU

Abstract. Since the pioneering work by Treloar, many models based on polymer chain statistics have been proposed to describe rubber elasticity. Recently, Alicandro, Cicalese, and the first author have rigorously derived a continuum theory of rubber elasticity from a discrete model by variational convergence. The aim of this paper is twofold. First we further physically motivate this model, and complete the analysis by numerical simulations. Second, in order to compare this model to the literature, we present in a common language two other representative types of models, specify their underlying assumptions, check their mathematical properties, and compare them to Treloar's experiments.

1. Introduction

Two theories at different scales allow us to describe rubber-like materials. The first and more classical one is the continuum mechanics framework, ideal rubbers being prototypical of hyperelastic materials in finite deformation. At the other end of the spectrum, we find statistical mechanics approaches for polymer chains. In the continuum theory of rubber elasticity, constitutive laws are phenomenological in essence, see for instance the survey article [5] (even if somewhat guided by the mathematical analysis, see [9]). In statistical mechanics, the free energy of a polymer chain can be derived from first principles, as in [12]. It is therefore tempting to relate the *adhoc* energy densities encountered at the continuum level with the physically motivated (free) energy of polymer chains. The difficulty of such a program is to pass from the free energy of one polymer chain to the free energy of a network of *cross-linked* polymer chains.

A constitutive assumption is usually made to pass from the polymer chain to the polymer network. The easiest and first assumption is due to Treloar in [28] and consists in imposing that the network deforms locally in an affine manner. Hence all the polymer chains are deformed according to the macroscopic strain gradient. This is the so-called *affine assumption* (or in another context the *Cauchy-Born rule*). Another type of assumption consists in postulating a geometric response of a representative volume element of polymer chains (somewhat unrelated to the actual polymer network). The eight-chain model by Arruda and Boyce in [4] is of this type. Amazingly, such models can be in good agreement with real experiments, even with a few free parameters.

Yet, the "most natural" assumption in a static setting is based on the minimization principle: the network "should" spontaneously relax its (free) energy given the imposed boundary conditions and external loads. In particular the deformation of the polymer chains inside the sample is given by the state which minimizes the overall energy of the network. In contrast to the other two types of models, such a constitutive assumption makes it impossible to directly obtain analytical formulas for the effective constitutive relations. This is clearly a handicap for practical purposes — see however [10] for a possible strategy to circumvent this difficulty. In [8], Böl and Reese have proposed in this context a finite element modeling of rubber based on polymer chain statistics. As proved in [1, 3, 2], the approach by Böl and Reese is consistent with continuum mechanics at the limit when the size of the mesh goes to zero. There is a conceptual gap in this passage to the limit, which gives rise to what we call the variational model. This does not appear in [8].

Date: February 23, 2012.

The aim of the present work is to describe the different models mentioned above, and properly define the variational model. In particular, we make precise their underlying assumptions, compare them, and possibly identify the regimes where they may coincide. The paper is organized as follows. In Section 2 we describe the Treloar, the Arruda-Boyce, and the Böl-Reese models, whereas the variational model is motivated and precisely defined in Section 3. We then address the main mechanical and mathematical properties of the models in Section 4. For the Treloar and the Arruda-Boyce models, analytical formulas can be obtained in terms of the principal invariants of the Cauchy-Green strain tensor. For the variational model, one has to appeal to numerical simulations. The numerical solution method and some convergence issues are analyzed in Section 5. The last section is dedicated to a quantitative comparison of the different models on Treloar's data, starting with the same characteristic parameters at the polymer-chain level.

Throughout the text we use the following notation:

- $\{\mathbf{e}_1, \mathbf{e}_2, \mathbf{e}_3\}$ denotes the canonical basis of $\mathbb{R}^3$;
- $\mathbb{M}^3$ is the set of 3×3 real matrices (strain gradients in $\mathbb{R}^3$), and $\mathbb{M}^3_+$ is the subset of those matrices with positive determinants;
- For all $\xi \in \mathbb{M}^3$, $I_1(\xi)$, $I_2(\xi)$, and $I_3(\xi)$ denote the first, second, and third principal invariants of $\xi^T\xi$, respectively, that is:
$$I_1(\xi) := \mathrm{tr}(\xi^T\xi),\ I_2(\xi) := \mathrm{tr}(\mathrm{cof}(\xi^T\xi)),\ I_3(\xi) = (\det \xi)^2;$$
- $SO(3)$ is the set of rotations of $\mathbb{R}^3$;
- S^2 is the unit sphere in $\mathbb{R}^3$;
- D is an open bounded domain with a Lipschitz boundary;
- For all $1 < p < +\infty$, $L^p(D)$, $W^{1,p}(D)$, and $W^{1,p}_0(D)$ denote the Lebesgue space of p-integrable functions on D, the Sobolev space of p-integrable functions on D whose distributional gradients are also p-integrable in D, and the Sobolev space of such functions which additionally vanish on the boundary ∂D of D, respectively.

2. Review of some discrete models for rubber

Before introducing the discrete models, we first quickly review the polymer chain free energies usually used as a fundamental brick in the polymer chain models.

2.1. Polymer chain free energy.

Given a polymer chain made of N rigid segments of length l at absolute temperature $\beta = \frac{1}{k_B T}$, with a chain density n, the free energy (of entropic origin) for a chain of length r_c can be modeled by

$$\tilde{W}_c(r_c, N) = \frac{n}{\beta} N \left(\frac{r_c}{Nl} \theta\left(\frac{r_c}{Nl}\right) + \log \frac{\theta\left(\frac{r_c}{Nl}\right)}{\sinh \theta\left(\frac{r_c}{Nl}\right)} \right) - \frac{c}{\beta}, \tag{1}$$

where c is a constant and θ the inverse of the Langevin function $\mathcal{L} : \alpha \mapsto \coth \alpha - \frac{1}{\alpha}$. The energy (1) has been derived by Kuhn and Grün in [21] using a non-Gaussian assumption: each segment of the chain obeys a non-Gaussian random walk. We refer to [12] for details. In particular, the energy is infinite as soon as $r_c > Nl$, the total length of the chain. For discrete to continuum derivations, θ is usually replaced by the first terms of its series expansion:

$$\theta(r) = 3r + \frac{9}{5} r^3 + \frac{297}{175} r^5 + \frac{1539}{875} r^7 + \frac{672}{359} r^9 + O(r^{11}), \tag{2}$$

although this simplification is not essential for our discussion (e.g. Padé approximations behave better close to the finite extensibility limit). A series expansion of $\tilde{W}_c$ then reads:

$$\begin{aligned} \tilde{W}_c(r_c, N) \ = \ & \frac{n}{\beta} N \left[\frac{3}{2} \left(\frac{r_c}{Nl}\right)^2 + \frac{9}{20} \left(\frac{r_c}{Nl}\right)^4 + \frac{9}{350} \left(\frac{r_c}{Nl}\right)^6 + \frac{81}{7000} \left(\frac{r_c}{Nl}\right)^8 \right. \\ & \left. + \frac{243}{673750} \left(\frac{r_c}{Nl}\right)^{10} \right] + O\left(\left(\frac{r_c}{Nl}\right)^{12} \right). \end{aligned} \tag{3}$$

The behavior of the polynomial approximation at infinity satisfies the classical coercivity assumption on hyperelastic materials at infinity. Replacing the inverse of the Langevin function by the first terms of a series expansion is a rather good modeling at high temperature (see [23]). A remarkable property of such an energy is $\tilde{W}_c(0) = 0$ and $\tilde{W}_c(1) > 0$. In particular the prefered configuration of a polymer chain satisfies $r_c = 0$.

When N is fixed, we simply write $\tilde{W}_c(r_c)$ instead of $\tilde{W}_c(r_c, N)$.

2.2. **Treloar type models.** The variant of the Treloar model we consider here is the following. As in [28], we assume that the polymer network deforms in an affine manner. We also assume that the network is isotropic and we give ourselves a distribution function $\nu(N)$ of the polymer chains made of N segments in the network. We then associate general energies with the polymer chains, such as the one recalled in the previous subsection. To make precise the reference configuration of the chains, we use a distribution function $\rho(L, N)$ which gives the probability that a chain made of N segments has length L in the reference configuration. This yields for all $\xi \in \mathbb{M}^3$,

$$\tilde{W}_{\mathrm{T}}(\xi) \quad = \quad \int_{\mathbb{R}^+} \int_{\mathbb{R}^+} \int_{S^2} \tilde{W}_c(L|\xi \cdot e(X)|, N) d\sigma(X) d\rho(L, N) d\nu(N),$$

where S^2 is the unit sphere centered at the origin O, $e(X)$ is the vector OX for $X \in S^2$, and σ is the uniform measure on S^2.

In what follows, for simplicity, we assume there is only one type of chains in the network (that is, all the chains have a fixed number N of segments), and we assume that the length of the polymer chains in the reference configuration is $\sqrt{N}l$, which corresponds to the average distance of a random walker from the origin after N steps of length l, see [12]. The Treloar energy density then turns into

$$\tilde{W}_{\mathrm{T}}(\xi) \quad = \quad \int_{S^2} \tilde{W}_c(\sqrt{N}l|\xi \cdot e(X)|) d\sigma(X). \tag{4}$$

When $\tilde{W}_c$ is replaced by its Taylor expansion (3) in (4), we denote by $\tilde{W}_{\mathrm{T}}^5$ the associated the Treloar model (that is a Taylor expansion of $\tilde{W}_{\mathrm{T}}$). As one can check on (4), $\tilde{W}_{\mathrm{T}}^5$ is minimal for $\xi = 0$. Actually one has not taken repulsion of chains into account in the model. To include volumetric effects in the description, one may add the so-called Helmholtz volumetric energy

$$W_{\mathrm{Helm}}(\xi) = K(\det(\xi)^2 - 1 - 2\log(\det(\xi))), \tag{5}$$

yielding

$$W_{\mathrm{T}}^5(\xi) = \tilde{W}_{\mathrm{T}}^5(\xi) + W_{\mathrm{Helm}}(\xi),$$

which is the final form we will consider. This could be generalized to any order p of the Taylor expansion.

2.3. **Arruda-Boyce type models.** In their original paper [4], Arruda and Boyce have proposed a model which relates the energy of the material in terms of its deformation gradient through the free energy of polymer chains. This model is called the eight-chain model. It basically amounts to taking as a representative volume element for the polymer network the set of eight chains linking the center of a cube to its eight corners. For a deformation gradient $\xi \in \mathbb{M}^3_+$, the cube is supposed to align itself according to the principal directions of the deformation (eigenvectors of $\xi^T\xi$), and to deform itself according to the principal stretches (square root of the eigenvalues of $\xi^T\xi$). The energy density of the material is then proportional to the energy of the chains in the deformed cube. Note that

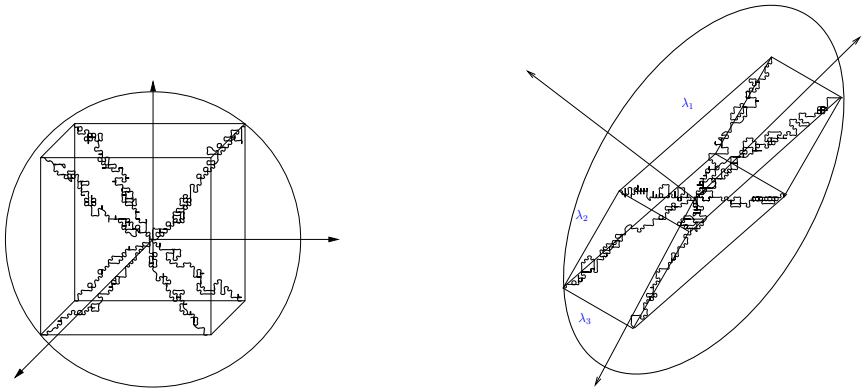

FIGURE 1. Arruda-Boyce model: undeformed and deformed representative element

each of the eight chains is deformed by the ratio $\sqrt{\frac{I_1(\xi)}{3}}$, where $I_1(\xi) = \mathrm{tr}(\xi^T\xi)$ is the first principal invariant. For isochoric deformations, the energy density is thus given by

$$\begin{aligned}\tilde{W}_{\mathrm{AB}}(\xi) &= \frac{n}{\beta}N\left(\sqrt{\frac{I_1(\xi)}{3}}\frac{\sqrt{N}l}{Nl}\theta(\sqrt{\frac{I_1(\xi)}{3}}\frac{\sqrt{N}l}{Nl}) + \log\left(\frac{\theta(\sqrt{\frac{I_1(\xi)}{3}}\frac{\sqrt{N}l}{Nl})}{\sinh\theta(\sqrt{\frac{I_1(\xi)}{3}}\frac{\sqrt{N}l}{Nl})}\right)\right)\\ &= \frac{n}{\beta}N\left(\sqrt{\frac{I_1(\xi)}{3N}}\theta(\sqrt{\frac{I_1(\xi)}{3N}}) + \log\left(\frac{\theta(\sqrt{\frac{I_1(\xi)}{3N}})}{\sinh\theta(\sqrt{\frac{I_1(\xi)}{3N}})}\right)\right). \qquad (6)\end{aligned}$$

where typically $\frac{n}{\beta} = 0.27$ and $N = 26.5$ to fit Treloar's experiments. As for the Treloar model, when $\tilde{W}_c$ is replaced by its Taylor expansion up to order p (see (3) for $p = 5$), this gives rise to a Taylor expansion of (6) that we denote by $\tilde{W}^p_{\mathrm{AB}}$.

In order to consider non isochoric deformations, one should add the Helmholtz volumetric energy as for the Treloar type energies. We thus set

$$W^p_{\mathrm{AB}}(\xi) = \tilde{W}^p_{\mathrm{AB}}(\xi) + W_{\mathrm{Helm}}(\xi). \qquad (7)$$

This variant of the Arruda-Boyce model is not the most commonly encountered. One usually uses reduced invariants:

$$\bar{W}^p_{\mathrm{AB}}(\xi) = \tilde{W}^p_{\mathrm{AB}}((\det\xi)^{-1/3}\xi) + W_{\mathrm{Helm}}(\xi), \qquad (8)$$

which amounts to assuming that the energy density can be additively split into an isochoric part and a volumetric part. The advantage of such a decomposition is that the identity is once more the unique natural state of the energy density. Recalling however how the model has been built, it may seem more natural to take into account changes of volume in the representative volume element itself, as it is done in (7). Yet, due to the value of K in (5) (which measures the strength of the volumetric energy), which may be typically 10^4 times larger than $\frac{n}{\beta} \sim 0.1$, the difference is not substantial in practice.

2.4. **Böl-Reese model.** The model developed by Böl and Reese in [8] is a hybrid model at the macroscopic scale. In particular, the energy of a macroscopic sample D is associated with a tetrahedral mesh of D: it is the combination of a volumetric energy on each element T of the mesh (typically the Helmholtz energy) and an energy associated with the edges of the mesh, which model "bundles" of polymer chains. The energy of one edge is given by a constant times the energy $\tilde{W}_c(r)$ in (3), where $r = \frac{L}{L_0}$, L_0 is the length of the edge in the reference configuration, and L, the length of the edge in the deformed configuration. The other parameters in $\tilde{W}_c$ are then to be fitted.

This model is hybrid since it does not enter the classical framework of continuum mechanics: the macroscopic energy is split into a continuous volumetric energy, and a discrete energy associated with edges of a mesh. As shown in [7], numerical experiments are in good agreement with other classical models and experimental data. Yet this does not provide a pure continuous description of rubber elasticity. As proved in [3], the model "converges" to a continuous model as the meshsize goes to zero. However, the limiting model highly depends on the geometry of the mesh in terms of isotropy properties for instance. This issue was not addressed in [7, 8].

The model we propose in the following section coincides with the limit of the Böl-Reese model as the meshsize goes to zero for a suitable mesh. It will therefore not be surprising that the two models yield similar results. Nevertheless, our modeling assumptions are different: we do not need to introduce bundles of polymer chains, and only rely on a statistical mechanics approach.

3. Variational model: Motivation and rigorous results

3.1. **Description and motivation.** We consider a macroscopic sample of natural rubber D, whose boundary is linearly deformed through the map $x \mapsto \xi \cdot x$, $\xi \in \mathbb{M}^3_+$. The sample is made of a network of cross-linked polymer chains. The cross-links are assumed to be permanent. In this first (rough) model, we neglect entanglements, that is, we neglect topological constraints (this will be made clear in the definition of the network). Each polymer chain is itself made of a given number of monomers: for a chain the energy of a configuration is obtained through the probability density of a random walk (see for instance [21], [28]). We assume that each monomer is surrounded by a fixed volume (from which other monomers are excluded), and that the network of chains is packed and almost incompressible. This assumption adds a volumetric term to the energy which depends on the configuration of the network. This volumetric term accounts for the interaction between the chains (which does not appear in the energy of one single chain). Note that the relevant scale associated with this contribution is much smaller than the one corresponding to the contribution associated with the random walk variable.

In the description of the rubber model we consider, we denote by u the positions of the cross-links, and by $s = \{s_i\}$ the positions of the monomers of the chain i. The Hamiltonian of the system can be split into two parts:

$$H(u, s) = H_{\text{vol}}(u, s) + \sum_i H_i(u, s_i).$$

The first part $H_{\text{vol}}(u, s)$ is the volumetric energy of the network, which models the interactions between the chains, whereas the second part $H_i(u, s_i)$ is the energy of each chain as if it were isolated (and for which u prescribes the end-to-end vector, and s_i describes the positions of the monomers constituting the chain).

At finite temperature $\beta = \frac{1}{k_B T}$, the Gibbs distribution yields the following formula for the free energy of a given deformed network:

$$\begin{aligned} F(\xi, D) &= -\frac{1}{\beta} \ln Z \\ &= -\frac{1}{\beta} \ln \left[\int_U \int_{\prod S_i(u)} \exp\left(-\beta H_{\text{vol}}(u, s) - \sum_i \beta H_i(u, s_i) \right) du \prod_i ds_i \right], \end{aligned}$$

where Z is the partition function, U is the set of admissible positions of the cross-links (satisfying the constraint on the boundary), and $S_i(u)$ denotes the set of admissible positions of the monomers composing the chain i whose head and tail are prescribed by u.

This free energy is far from being explicit. However, it is possible to further simplify the problem and still capture some interesting features. We present a heuristic argument which leads to the decoupling of the s_i variables. We first assume that $H_{\rm vol}(u,s) = H_{\rm vol}(u)$ only depends on u and not on s, which amounts to replacing the excluded volume constraint around monomers by an excluded volume constraint between cross-links. Note that this is a rather strong assumption whose effect is to make chains interact via their cross-links only: this decouples the variables s_i from one another. We may then rewrite the free energy as follows:

$$\begin{aligned} F(\xi,D) \;&=\; -\frac{1}{\beta}\ln\Big[\int_U \exp\Big(-\beta H_{\rm vol}(u) \\ &\qquad +\beta\sum_i \frac{1}{\beta}\ln\Big[\int_{S_i(u)}\exp\Big(-\beta H_i(u,s_i)\Big)ds_i\Big]\Big)du\Big]. \end{aligned}$$

Assuming that the volumetric term is dominant and very stiff away from isochoric deformations u, one may restrict the integration over deformations $u \in U$ which "almost preserve the local volume". We denote by $U_{\rm iso}$ this subset of U, and rewrite the assumption in the form

$$\begin{aligned} &\int_U \exp\Big(-\beta H_{\rm vol}(u) + \beta\sum_i \frac{1}{\beta}\ln\Big[\int_{S_i(u)}\exp\Big(-\beta H_i(u,s_i)\Big)ds_i\Big]\Big)du \\ &\qquad \simeq \int_{U_{\rm iso}} \exp\Big(-\beta H_{\rm vol}(u) + \beta\sum_i \frac{1}{\beta}\ln\Big[\int_{S_i(u)}\exp\Big(-\beta H_i(u,s_i)\Big)ds_i\Big]\Big)du. \quad (9) \end{aligned}$$

We expect the effective Hamiltonian

$$H_\xi(u,\beta) \;:=\; H_{\rm vol}(u) - \sum_i \frac{1}{\beta}\ln\Big[\int_{S_i(u)}\exp\Big(-\beta H_i(u,s_i)\Big)ds_i\Big]$$

to be coercive on $U_{\rm iso}$ in the sense that there exist a minimizer $\bar u(\xi,\beta) \in U_{\rm iso}$ and a symmetric positive definite matrix $K(\xi,\beta)$ (whose size coincides with the number N of cross-links in D) such that for all $u \in U_{\rm iso}$, we have

$$H_\xi(u,\beta) - H_\xi(\bar u(\xi,\beta),\beta) \;\geq\; \frac{1}{2}(u-\bar u(\xi,\beta))\cdot K(\xi,\beta)(u-\bar u(\xi,\beta)). \quad (10)$$

Let us discuss this assumption. Although this inequality may seem to require the convexity of H with respect to u, it does not. In particular, if one thinks in terms of nonlinear elasticity, replace u by a deformation field in D, and H by an integral functional of the form $\int_D W(\nabla u(x))dx$, then $\bar u(\xi,\beta)$ would simply be $x \mapsto \xi\cdot x$, and (10) would hold locally as a consequence of:

- quasiconvexity,
- isotropy,
- strong ellipticity (that is, strict rank-one convexity, and not the stronger property of convexity)

of W. This is related to the non-negativity of the second variation of W in the class of functions which vanish on the boundary of D.

Using assumption (9) we rewrite $F(\xi,\beta)$ as

$$\begin{aligned} F(\xi,D) &\approx -\frac{1}{\beta}\ln\left[\int_{U_{\rm iso}}\exp\Big(-\beta H_\xi(u,\beta)\Big)du\right] \\ &= -\frac{1}{\beta}\ln\left[\exp\Big(-\beta H_\xi(\bar u(\xi,\beta),\beta)\Big)\right. \\ &\qquad\left.\times\int_{U_{\rm iso}}\exp\Big(-\beta\big(H_\xi(u,\beta)-H_\xi(\bar u(\xi,\beta),\beta)\big)\Big)du\right] \\ &= H_\xi(\bar u(\xi,\beta),\beta)-\frac{1}{\beta}\ln\left[\int_{U_{\rm iso}}\exp\Big(-\beta\big(H_\xi(u,\beta)-H_\xi(\bar u(\xi,\beta),\beta)\big)\Big)du\right]. \end{aligned}$$

In order to show that $H_\xi(\bar u(\xi,\beta),\beta)$ is a good approximation of $F(\xi,D)$ we appeal to assumption (10):

$$\begin{aligned} &|F(\xi,D)-H_\xi(\bar u(\xi,\beta),\beta)| \\ &\le \left|\frac{1}{\beta}\ln\left[\int_{U_{\rm iso}}\exp\Big(-\beta\big(H_\xi(u,\beta)-H_\xi(\bar u(\xi,\beta),\beta)\big)\Big)du\right]\right| \\ &\le \left|\frac{1}{\beta}\ln\left[\int_{U_{\rm iso}}\exp\Big(-\frac{\beta}{2}(u-\bar u(\xi,\beta))\cdot K(\xi,\beta)(u-\bar u(\xi,\beta))\Big)du\right]\right| \\ &\le \left|\frac{1}{\beta}\ln\left[\int_{\mathbb{R}^N}\exp\Big(-\frac{\beta}{2}u\cdot K(\xi,\beta)u\Big)du\right]\right|. \end{aligned}$$

Assuming further that there exists $k(\xi,\beta)>0$ (independent of N) such that $K(\xi,\beta)\ge k(\xi,\beta)\mathrm{Id}$ in the sense of symmetric matrices, the above inequality turns into

$$|F(\xi,D)-H_\xi(\bar u(\xi,\beta),\beta)| \le \frac{N}{2\beta}\ln\Big(\beta k(\xi,\beta)\Big).$$

Since the number N of cross-links is proportional to $|D|$, and provided $k(\xi,\beta)$ remains of order one, this yields

$$\left|\frac{F(\xi,D)}{|D|}-\frac{\inf_{u\in U_{\rm iso}}H_\xi(u,\beta)}{|D|}\right| \lesssim \frac{1}{\beta}\ln(\beta) = o(1), \tag{11}$$

for $\beta\gg 1$ (that is for small to moderate temperatures). Let us be more precise: a small to moderate temperature is a temperature for which

$$\frac{1}{\beta}\left|\frac{\partial k(\xi,\beta)}{\partial\xi}\right| \ll \frac{1}{|D|}\left|\frac{\partial H_{\rm vol}(\bar u)}{\partial\bar u}\frac{\partial\bar u(\xi,\beta)}{\partial\xi}\right|.$$

Indeed this inequality is not restrictive since $H_{\rm vol}$ is supposed to be stiff, and it implies (11).

We have therefore given a heuristic argument for the free energy identification

$$\frac{F(\xi,D)}{|D|} \simeq \frac{\inf_{u\in U_{\rm iso}}H_\xi(u,\beta)}{|D|}. \tag{12}$$

Without anticipating too much, it is worth mentioning that the key assumption (10) does not only yield (12), but also implies that the homogenized material is strongly elliptic (see [14]). Conversely, the strong ellipticity of the model (which we observe numerically) is a strong sign in favor of assumption (10).

This heuristic argument justifies to treat polymer-chains at finite temperature (the sum of the free energies of the polymer chains at temperature T appear inside the infimum), and the cross-links at zero temperature (we take the infimum instead of the Gibbs distribution). In terms of orders of magnitude, recall that polymer chains are typically $100nm$ long

whereas the macroscopic sample is of the order of the cm, which yields a factor 10^5. Hence, provided D is a macroscopic sample, (12) will be close to the "thermodynamic limit"

$$W_{\rm V}(\xi) := \lim_{|D|\to\infty} \frac{F(\xi, D)}{|D|}, \tag{13}$$

where D properly invades $\mathbb{R}^3$ (see for instance [27]). For such a limit to exist, the network of polymer chains should have some ergodic property: either the network has some periodic structure (yet we are not dealing with crystals), or the network should yield spatial decorrelations (in a statistical or stochastic framework) — although other less physically relevant properties could also be considered stricto sensu.

Such a limiting process has been studied in [1, 2]. There, the limit (13) is proved to exist provided the stochastic network satisfies some structural and statistical properties. In addition, the link between boundary value problems associated with the network and boundary value problems with the energy density $W_{\rm V}$ is also made rigorous, thus generalizing the validity of the thermodynamic limit when boundary conditions and forcing terms (loads) are taken into account. We recall the relevant results in the following subsection.

3.2. **Homogenization of stochastic discrete systems.** In order to present the results of [2] on the homogenization of stochastic discrete systems, we need to define the notion of stochastic network, and make precise the associated energy functional.

Definition 1. *We say that a stochastic point process $\mathcal{L}$ in $\mathbb{R}^3$ (that is a sequence of random points in $\mathbb{R}^3$) is admissible if:*

- *(regularity) There exist $\mathbf{r} \geq r > 0$ such that almost surely:*
  - *any two points of $\mathcal{L}$ cannot be closer than r,*
  - *any ball of radius $\mathbf{r}$ contains at least one point of $\mathcal{L}$;*
- *(stationarity) $\mathcal{L}$ and $x + \mathcal{L}$ have the same statistics for all $x \in \mathbb{R}^3$;*
- *(ergodicity) $\mathcal{L}$ is ergodic.*

We further assume that the Delaunay tessellation $\mathcal{T}$ of $\mathbb{R}^3$ into tetrahedra associated with $\mathcal{L}$ (that is, the vertices of $\mathcal{T}$ are given by $\mathcal{L}$) is almost surely unique (see [11]*).*

For rigorous definitions of admissible stochastic lattices and their Delaunay tessellations, we refer the reader to [2], and to the references therein. Let us also introduce a rescaling of $\mathcal{L}$ and $\mathcal{T}$. For all $\varepsilon > 0$, we set $\mathcal{L}_\varepsilon := \varepsilon\mathcal{L}$, which satisfies Definition 1 with εr and $\varepsilon\mathbf{r}$ in place of r and $\mathbf{r}$, and with $\mathcal{T}_\varepsilon := \varepsilon\mathcal{T}$ in place of $\mathcal{T}$.

Given a tessellation $\mathcal{T}_\varepsilon$ of $\mathbb{R}^3$, one may define the space $\mathcal{S}(\mathcal{T}_\varepsilon)$ of continuous and piecewise affine deformations u_ε on $\mathcal{T}_\varepsilon$. Such deformations u_ε are such that their gradient ∇u_ε is piecewise contant on $\mathcal{T}_\varepsilon$. In particular, for every element T_ε (tetrahedron) of the tessellation $\mathcal{T}_\varepsilon$, $\det \nabla u_{\varepsilon|T_\varepsilon}$ measures the ratio of volume between $u_\varepsilon(T_\varepsilon)$ and T_ε.

We are now in position to associate an energy with any deformation field $u_\varepsilon \in \mathcal{S}(\mathcal{T}_\varepsilon)$, on an open bounded domain D of $\mathbb{R}^3$. We consider two contributions: an energy associated with the changes of length of the edges of the tessellation, and an energy associated with the changes of volume of the elements of the tessellation. More precisely, denoting by $\mathcal{E}$ the set of edges of $\mathcal{T}$, we define the energy of $u_\varepsilon \in \mathcal{S}(\mathcal{T}_\varepsilon)$ on D by

$$\begin{aligned} F_\varepsilon(u_\varepsilon, D) &= \varepsilon^3 \sum_{e\in\mathcal{E}, e\subset D/\varepsilon} W_{nn}\Big(|e_1 - e_2|, \frac{|u_\varepsilon(\varepsilon e_1) - u_\varepsilon(\varepsilon e_2)|}{\varepsilon|e_1 - e_2|}\Big) \\ &\quad + \sum_{T\in\mathcal{T}, T\subset D/\varepsilon} |\varepsilon T| W_{\rm vol}(\det \nabla u_{\varepsilon|\varepsilon T}), \end{aligned} \tag{14}$$

where $e = (e_1, e_2)$ (e_1 and e_2 are the two vertices of the edge e), $W_{nn} : \mathbb{R}^+ \times \mathbb{R}^+ \to \mathbb{R}^+$ is the energy of the deformed edges, and $W_{\rm vol} : \mathbb{R} \to \mathbb{R}^+$ is the volumetric energy. We make the following assumptions on W_{nn} and $W_{\rm vol}$:

Hypothesis 1. *There exist $p > 1$ and positive constants c, C such that for all $r \le \gamma \le \mathbf{r}$, $\lambda \ge 0$, and $\xi \in \mathbb{M}^3$,*

$$c\lambda^p - 1/c \;\le\; W_{nn}(\gamma, \lambda) \;\le\; C(\lambda^p + 1), \tag{15}$$

$$W_{\mathrm{vol}}(\det \xi) \;\le\; C(|\xi|^p + 1). \tag{16}$$

We then have the following convergence result (see [2, Theorem 5]).

Theorem 1. *For all $\varepsilon > 0$, let $\mathcal{L}_\varepsilon$ and $\mathcal{T}_\varepsilon$ be the rescaled stochastic point process and associated Delaunay tessellation of Definition 1. For every open bounded subset D of $\mathbb{R}^3$, we consider the energy $F_\varepsilon(u_\varepsilon, D)$ defined by (14) for $u_\varepsilon \in \mathcal{S}(\mathcal{T}_\varepsilon)$, and extended by $+\infty$ on $W^{1,p}(D) \setminus \mathcal{S}(\mathcal{T}_\varepsilon)$, for $p > 1$, W_{nn}, and W_{vol} as in Hypothesis 1.*
Then the functional $F_\varepsilon(\cdot, D)$ $\Gamma(L^p(D))$-converges on $W^{1,p}(D)$ as $\varepsilon \to 0$ to the functional $F_V(\cdot, D)$ defined by

$$F_{\mathrm{V}}(u, D) \;=\; \int_D W_{\mathrm{V}}(\nabla u(x))\, dx, \tag{17}$$

where $W_V : \mathbb{M}^d \to \mathbb{R}^+$ is quasiconvex, satisfies a standard growth condition of order p:

$$\text{there exists } C > 0 \text{ such that for all } \xi \in \mathbb{M}^d,\ \frac{1}{C}|\xi|^p - 1 \;\le\; W_V(\xi) \;\le\; C(1 + |\xi|^p),$$

and it is given by the asymptotic homogenization formula

$$W_{\mathrm{V}}(\xi) \;=\; \lim_{R\to\infty} \frac{1}{R^3} \inf\{F_1(u, Q_R), u \in \mathcal{S}(\mathcal{T}), u(x) = \xi \cdot x \text{ if } \mathrm{dist}(x, \partial Q_R) \le 2\mathbf{r}\}, \tag{18}$$

with $Q_R = (-R/2, R/2)^3$, almost surely.
In addition, if $\mathcal{L}$ is isotropic in the sense that for all rotations $\mathcal{R} \in SO(3)$, $\mathcal{L}$ and $\mathcal{R}(\mathcal{L})$ have the same statistics, then W_{V} is an isotropic energy density.

Remark 1. *Note that we can take spheres in place of cubes in the asymptotic formula (18), which we actually do in numerical approximations.*

Let us comment on Theorem 1. First, (18) is a mathematical version of (13), that shows the existence of the thermodynamic limit. It does not only provide the existence of W_{V}, but also gives some additional properties, such as quasiconvexity and isotropy. Second, from this Γ-convergence result (and its generalization to the case when Dirichlet boundary conditions are considered, see [2]), we deduce that given a boundary value problem on D and a minimizer u_ε of the discrete energy at scale $\varepsilon > 0$, u_ε converges in $L^p(D)$ as $\varepsilon \to 0$ to a minimizer $u \in W^{1,p}(D)$ of the continuous energy with energy density W_{V}, the same boundary conditions, and external loads. This fully justifies the passage to the limit as $\varepsilon \to 0$ in the static setting: not only the energy does converge, but also the minimizers.

In the following subsection, we show how to apply Theorem 1 to the discrete model introduced in Subsection 3.1, in order to define the variational model and its energy density W_{V}.

3.3. **Discrete variational model.** In order to make use of the rigorous results recalled above, we need to put (12) in the form of (14). To this aim, we further assume that the network is a tessellation of D into tetrahedra whose edges are the polymer chains, so that we can write (12) in the form

$$F(\xi, D) \;\approx\; \inf_{u\in U} \{F_{\varepsilon_0}(u_{\varepsilon_0}, D)\},$$

for some $\varepsilon_0 > 0$, some function set U related to $\xi \in \mathbb{M}^3$, and with F_{ε_0} as in (14). The parameter ε_0 is the intrinsic lengthscale of the polymer network, which is the length of a monomer, also denoted by l. An edge e of the tessellation at scale ε_0 is then supposed to be made of

$$N_e \;\simeq\; \left(\frac{|e|}{l}\right)^2 = \left(\frac{|e|}{\varepsilon_0}\right)^2$$

segments (or monomers). Hence, if the edge e has length L after deformation, its free energy is given by

$$\begin{aligned}\tilde{W}_c(L,N_e) &= \frac{n}{\beta}N_e\left(\frac{L}{N_e l}\theta\left(\frac{L}{N_e l}\right)+\log\frac{\theta\left(\frac{L}{N_e l}\right)}{\sinh\theta\left(\frac{L}{N_e l}\right)}\right)\\ &= \frac{n}{\beta}\left(\frac{|e|}{\varepsilon_0}\right)^2\left(\frac{L\varepsilon_0}{|e|^2}\theta\left(\frac{L\varepsilon_0}{|e|^2}\right)+\log\frac{\theta\left(\frac{L\varepsilon_0}{|e|^2}\right)}{\sinh\theta\left(\frac{L\varepsilon_0}{|e|^2}\right)}\right).\end{aligned}$$

This formula allows us to properly define W_{nn}. First we rescale the network so that it is of order $\varepsilon = 1$. The rescaled network will be taken as a reference and denoted by $\mathcal{T}$. The associated parameters in Definition 1 are $r = 1$ (each chain has at least one monomer), and $\mathbf{r} \lesssim 10$ (a chain has, say, at most 100 monomers, so that its averaged length is of order 10). Let now $e = (e_1, e_2)$ be an edge of $\mathcal{T}$, and for $\varepsilon > 0$, let $u_\varepsilon \in \mathcal{S}(\mathcal{T}_\varepsilon)$, where $\mathcal{T}_\varepsilon$ is the ε-rescaled version of $\mathcal{T}$. Then, setting $\lambda := \frac{|u_\varepsilon(\varepsilon e_1)-u_\varepsilon(\varepsilon e_2)|}{\varepsilon|e_1-e_2|}$ the edge dilatation, the rescaled energy of the rescaled edge εe deformed by u_ε is given by

$$\begin{aligned}W_{nn}(|e|,\lambda) &= \frac{n}{\beta\varepsilon_0^3}|e|^2\left(\frac{\lambda|e|}{|e|^2}\theta\left(\frac{\lambda|e|}{|e|^2}\right)+\log\frac{\theta\left(\frac{\lambda|e|}{|e|^2}\right)}{\sinh\theta\left(\frac{\lambda|e|}{|e|^2}\right)}\right)\\ &= \frac{n}{\beta\varepsilon_0^3}|e|^2\left(\frac{\lambda}{|e|}\theta\left(\frac{\lambda}{|e|}\right)+\log\frac{\theta\left(\frac{\lambda}{|e|}\right)}{\sinh\theta\left(\frac{\lambda}{|e|}\right)}\right), \qquad (19)\end{aligned}$$

corresponding to the unscaled values of the energy of the polymer chains when $\mathcal{T}$ is ε_0-rescaled. For the volumetric energy, we take $W_{\rm vol}(\det\xi) = W_{\rm Helm}(\xi)$, where $W_{\rm Helm}$ is defined in (5).

It remains to check that W_{nn} and $W_{\rm vol}$ satisfy Hypothesis 1. In fact, the estimate from above is satisfied by W_{nn} provided we consider any order of the Taylor expansion of the inverse of the Langevin function (for instance (3), in which case $p = 10$). For the volumetric term, there is a technical difficulty: the Helmholtz energy density (5) does not satisfy Hypothesis 1 since $W_{\rm Helm}(\xi)$ blows up as $\det\xi \to 0$ (as it is desirable in nonlinear elasticity). Although the discrete homogenization theorem is expected to hold in this case as well, the current state-of-art does not allow to directly extend the result to this case. In order to circumvent this difficulty, we have proceeded in two steps in [2]. First we have regularized the behavior of $W_{\rm Helm}$ for $\det\xi \le \eta$ for η small so that the new volumetric energy density $W_{\rm vol}^\eta$ satisfies Hypothesis 1. We have then appealed to Theorem 1, which yields the existence of a homogenized energy density $W_{{\rm V},\eta}^p$ (with obvious notation for the order $2p$ of the Taylor expansion (3)). In a second step, we have let the regularization parameter η go to zero, and showed that $W_{{\rm V},\eta}^p$ converges to some energy density $W_{\rm V}^p$ (in the sense that the associated energy functionals Γ-converge) which satisfies in addition of frame-invariance, quasiconvexity, and weak lower-semicontinuity of the integral functional, the desired behavior

$$W_{\rm V}(\xi) \to +\infty, \qquad \text{if } \det\xi \to 0.$$

We refer the reader to [2, Theorem 11] for details. In the rest of this paper, the variational energy density $W_{\rm V}$ is defined as the energy density obtained by the double limit procedure of [2, Theorem 11] :

$$W_{\rm V}^p(\xi) = \lim_{\eta\to 0}\lim_{R\to\infty}\frac{1}{R^3}\inf\{F_1(u,B_R), u\in\mathcal{S}(\mathcal{T}), u(x) = \xi\cdot x \text{ if } \operatorname{dist}(x,\partial B_R)\le 2\mathbf{r}\},$$

with $B_R = \{Rx : |x| \le 1\}$, F_1 given by (14), W_{nn} given by the p-order expansion of (19), and $W_{\rm vol}$ by the η regularization of $W_{\rm Helm}$.

Remark 2. *As pointed out to us by François Lequeux, the assumption that the polymer network forms a tetrahedral tessellation of* $\mathbb{R}^3$ *is very strong. In particular it leads to a much too high connectivity of polymer chains. Therefore, the model is expected to overestimate the rigidity of the polymer network. In addition, as noticed by Michael Rubinstein, the density of monomers in the model is not correct: we have imposed local incompressibility whereas our model is not at the packing limit. Both issues are very important from a physical point of view and will be addressed in detail in a future paper* [17].

4. General properties

4.1. **Mechanical properties.** We now prove that the energy densities W_{T}, W_{AB} and W_{V} of the Treloar, Arruda-Boyce, and variational models all satisfy the following mechanical properties:

- hyperelasticity,
- frame-invariance,
- isotropy,
- blow up of the energy when $\det \xi \to 0^+$,
- strong ellipticity.

Hyperelasticity is obvious since the models only depend on the pointwise value of the strain gradient. Frame-invariance is a consequence of the dependence upon $\xi^T \xi$ for the three models (or upon distances at the discrete level).

Isotropy is postulated in (AB) since the representative element aligns itself with the principal directions of ξ. It is a consequence of the integration over all the directions for (T). For (V), one has to assume in addition that the stochastic network is isotropic in the mean (the expectation of the stochastic network is isotropic), which implies the isotropy of the energy density, as proved in [3, Theorem 6].

The behavior of the energy when $\det \xi \to 0^+$ is a direct consequence of the definition of W_{Helm} for (T) and (AB), whereas for (V) it is a consequence of the double limit procedure.

Strong ellipticity of the energy density implies two important properties: the material is stable (that is, homogeneous deformations are strict local minimizers), and this property allows one to prove short-time existence results for the system of elastodynamics. We recall that an energy density $W : \mathbb{M}^3 \to \mathbb{R}$ is elliptic if and only if for all $\xi \in \mathbb{M}^3$ and all $a, b \in \mathbb{R}^3$, the function $\mathbb{R} \to \mathbb{R}, t \mapsto W(\xi + ta \otimes b)$ is convex. We say that W is strongly elliptic if $t \mapsto W(\xi + ta \otimes b)$ is in addition α-elliptic for some $\alpha > 0$ (that is provided W is twice-differentiable: for all $\xi \in \mathbb{M}^3$, there exists $\alpha > 0$ such that $a \otimes b \cdot D^2 W(\xi) a \otimes b \geq \alpha |a \otimes b|^2$ for all $a, b \in \mathbb{R}^3$).

Lemma 1. *The functions* $\tilde{W}_{\mathrm{T}}$ *and* $\tilde{W}_{\mathrm{AB}}$ *are strongly elliptic on* $\mathbb{M}^3_+$.

Proof. We split the proof into two steps.

Step 1. Convexity of $\tilde{W}_c(\cdot, N)$.
We first claim that for all $N > 0$, the function $r \mapsto \tilde{W}_c(r, N)$ defined in (1) is convex, increasing, and α-elliptic with constant $\alpha = \frac{6n}{\beta N l^2}$ on $\mathbb{R}^+$.
The argument goes as follows. Since the Langevin function $\mathrm{La} : t \mapsto \coth t - \frac{1}{t}$ is concave and decreasing on $\mathbb{R}^+$, its inverse θ is convex and increasing. In addition, the function

$$t \mapsto \frac{\sinh t}{t}$$

is convex and increasing on $\mathbb{R}^+$. Hence,

$$r \mapsto \frac{\sinh \theta(r)}{\theta(r)}$$

is convex and increasing on $\mathbb{R}^+$ as well. Likewise, since

$$t \mapsto -\log t$$

is convex and increasing on $\mathbb{R}^+_* = (0, +\infty)$,

$$r \mapsto \log\left(\frac{\theta(r)}{\sinh\theta(r)}\right)$$

is convex and increasing on $\mathbb{R}^+$. The same argument holds for

$$r \mapsto r\theta(r).$$

In addition, its second derivative, given by

$$r \mapsto r\theta''(r) + 2\theta'(r),$$

is bounded by below by $2\theta'(r) \geq 6$ on $\mathbb{R}^+$ in view of the convexity of θ and using the series expansion (2) of θ. Taking into account the coefficients in (1) proves the claim.

Step 2. Strong ellipticity of $\tilde{W}_{\rm AB}$ and $\tilde{W}_{\rm T}$ on $\mathbb{M}^3_+$.
We first treat $\tilde{W}_{AB}$. From Step 1 and (6), we infer that $\tilde{W}_{AB}$ is convex on $\mathbb{M}^3$ since $\xi \mapsto \sqrt{I_3(\xi)}$ is convex as the Frobenius norm on $\mathbb{M}^3$. For all $i, j \in \{1, 2, 3\}$, we have

$$\begin{aligned}\mathbf{e}_i \otimes \mathbf{e}_j \cdot D^2_{\xi\xi}\tilde{W}_{\rm AB}(\xi)\mathbf{e}_i \otimes \mathbf{e}_j \\ = \tilde{W}_c'(\sqrt{I_1(\xi)})\mathbf{e}_i \otimes \mathbf{e}_j \cdot D^2_{\xi\xi}\sqrt{I_1}(\xi)\mathbf{e}_i \otimes \mathbf{e}_j + \tilde{W}_c''(\sqrt{I_1(\xi)})D_\xi\sqrt{I_1}(\xi) \otimes D_\xi\sqrt{I_1}(\xi).\end{aligned}$$

Since

$$\mathbf{e}_i \otimes \mathbf{e}_j \cdot D^2_{\xi\xi}\sqrt{I_1}(\xi)\mathbf{e}_i \otimes \mathbf{e}_j = \frac{I_1(\xi) - \xi_{ij}^2}{I_1(\xi)^{3/2}}$$

is positive for all $i, j \in \{1, 2, 3\}$ for $\det\xi \neq 0$, since $\tilde{W}_c'(\sqrt{I_1(\xi)}) > 0$ for $\xi \neq 0$, and since $\tilde{W}_c''(\sqrt{I_1(\xi)})D_\xi\sqrt{I_1}(\xi) \otimes D_\xi\sqrt{I_1}(\xi)$ is an elliptic tensor (although not strongly) for all $\xi \in \mathbb{M}^3$, the energy density $\tilde{W}_{\rm AB}$ is strongly elliptic on $\mathbb{M}^3_+$.

We now turn to $W_{\rm T}$ and proceed similarly. For all $e \in S^2$ the function $\xi \mapsto |\xi e|$ is convex by the triangle inequality. Hence, $\xi \mapsto \tilde{W}_c(|\xi e|)$ is a convex function as well, so that (4) implies that $W_{\rm T}$ is convex on $\mathbb{M}^3$ as a convex combination of convex functions (for e describing S^2). We now prove the strong ellipticity on $\mathbb{M}^3_+$. We have:

$$\int_{S^2} \mathbf{e}_i \otimes \mathbf{e}_j \cdot D^2_{\xi\xi}(|\xi e(X)|)\mathbf{e}_i \otimes \mathbf{e}_j d\sigma(X) = \int_{S^2} \frac{|\xi e(X)|^2 - (\mathbf{e}_i \cdot \xi e(X))^2}{|\xi e|^{3/2}} d\sigma(X)$$

which is positive provided $\xi \neq 0$. As above, this implies the strong ellipticity (of $\tilde{W}_{\rm T}$) on $\mathbb{M}^3_+$. □

In particular, $W_{\rm T}$ and $W_{\rm AB}$ are strongly elliptic as the sum of a strongly elliptic function on $\mathbb{M}^3_+$ ($\tilde{W}_{\rm AB}$ and $\tilde{W}_{\rm T}$, respectively) and of an elliptic function (the Helmholtz energy density, which is polyconvex and hence elliptic). The strong ellipticity of $W_{\rm V}$ is a much more delicate question, since strong ellipticity can be lost by homogenization in nonlinear elasticity (see in particular the very inspiring contribution of Geymonat, Müller, and Triantafyllidis in [13]). Provided some technical assumptions (which are supported by numerical simulations) and using the specific structure of $\tilde{W}_c$, the first author has shown in [14] that W_V is strongly elliptic on $\mathbb{M}^3_+$.

The following lemma shows that $W_{\rm T}$ and $W_{\rm AB}$ are coercive energy densities:

Lemma 2. *For all $p \geq 1$, the energy densities $\xi \mapsto W^p_{\rm AB}(\xi)$ and $\xi \mapsto W^p_{\rm T}(\xi)$ are the sum of a convex function of ξ and of a convex function of $\det\xi$. In addition, they satisfy the following coercivity property: there exists $c_p > 0$ such that for all $\xi \in \mathbb{M}^3$*

$$\min\{W^p_{\rm AB}(\xi), W^p_{\rm T}(\xi)\} + 1 \geq c_p(|\xi|^{2p} + |\det\xi|^2). \tag{20}$$

Proof. The structure of $W_{\rm AB}$ and $W_{\rm T}$ with respect to convexity is a consequence of the convexity of $\tilde{W}_{\rm AB}$ and $\tilde{W}_{\rm T}$ and of the convexity of the function $t \mapsto t^2 - 1 - 2\ln t$ on $\mathbb{R}_*^+$ (for the Helmholtz energy density defined in (5)).

The coercivity estimate (20) follows from the Helmholtz energy density, noting that

$$t^2 - 1 - 2\ln t \;\geq\; \max\left\{0, \frac{t^2}{2} - 2\right\},$$

and from the fact that the Taylor expansion (3) of $\tilde{W}_c$ only has non-negative coefficients for all $p \geq 1$. In particular,

$$\tilde{W}_{\rm AB}^p(\xi) \;\geq\; C_{\rm AB}(N,p)\sqrt{I_1(\xi)}^{2p} \;=\; C(N,p)|F|^{2p},$$

where $C_{\rm AB}(N,p)$ is a positive constant depending only on N and p, and $|\cdot|$ is the Frobenius norm on $\mathbb{M}^3$. For the Treloar model, we slightly anticipate on Section 6, and appeal to (24), that is $W_{\rm T}(\xi) \geq W_{\rm AB}(\xi)$ for all $\xi \in \mathbb{M}^3$. □

We conclude this subsection by the determination of the natural states of $W_{\rm T}$, $W_{\rm AB}$, and $W_{\rm V}$ (that is, the absolute minimizers of these energy densities on $\mathbb{M}^3_+$). In the case when reduced invariants are used, as for the original Arruda-Boyce model $W^{\rm AB}$ defined in (8), the absolute minimizer is the identity. When standard invariants are used, as in the variants of Arruda-Boyce and Treloar $W_{\rm AB}$ and $W_{\rm T}$ considered here, the identity is not the natural state since there is a competition between the energy of the polymer chains (which is minimized at 0) and the Helmholtz energy (which is minimized at identity). This gives rise to:

Lemma 3. *The energy densities $W_{\rm AB}$ and $W_{\rm T}$ admit the same unique natural state on $\mathbb{M}^3_+$, which is a dilatation αId with $0 < \alpha < 1$.*

Proof. This is a consequence of convexity. The functions $W_{\rm AB}$ and $W_{\rm T}$ are continuous on $\mathbb{M}^3_+$ and infinite at infinity and when $\det\xi \to 0^+$, so that they attain their minimum. Let α^3 denote the determinant of a minimizer. By frame-invariance it is enough to consider diagonal matrices of the form $\xi_{\lambda_1,\lambda_2,\alpha} := \mathrm{diag}(\lambda_1, \lambda_2, \alpha^3/(\lambda_1\lambda_2))$. The function $(\lambda_1,\lambda_2) \mapsto \tilde{W}_{\rm AB}(\xi_{\lambda_1,\lambda_2,\alpha})$ is strictly convex on $\mathbb{R}^2$ as the composition of an increasing strictly convex function with a strictly convex function. Hence it admits a unique minimum $(\lambda_1^*, \lambda_2^*)$. By symmetry, $\lambda_1^* = \lambda_2^*$, and therefore $\lambda_1^* = \lambda_2^* = \alpha$, and the natural state of determinant α^3 is the dilatation $\alpha\mathrm{Id}$. It remains to note that the function $t \mapsto W_{\rm AB}(t\mathrm{Id})$ is strictly convex, so that there is only one dilatation of minimal energy, and therefore only one natural state. The same arguments hold for $W_{\rm T}$, and the natural states coincide since $W_{\rm T}$ and $W_{\rm AB}$ coincide on dilatations. □

A weaker result holds for $W_{\rm V}$, based on [24, Theorem A]:

Lemma 4. [3, Theorem 8] *If $W_{\rm V}$ is isotropic (which follows from the isotropy of the stochastic lattice), it admits a natural state on $\mathbb{M}^3_+$ which is a dilatation.*

Note that uniqueness of the natural state is not ensured by this lemma (its proof only relies on argument which are compatible with the existence of several natural states, see [24, Section 3] e.g.).

Remark 3. *All the results of this paragraph hold as well for $W_{\rm AB}^p$, $W_{\rm T}^p$, and $W_{\rm V}^p$ for all $p \geq 1$ since the Taylor expansion (3) of $\tilde{W}_c$ is strictly convex at any order.*

4.2. **Boundary value problems.** The main interest of constitutive laws is their application to mechanical problems, or more mathematically to the associated boundary value problems. This section is devoted to the study of the well-posedness of boundary value problems in terms of minimization. Within this context, we only have to check classical coercivity and lower-semicontinuity properties ([6],[9]).

In particular we have the following (standard) existence result for the minimization problems associated with Treloar, Arruda-Boyce, and variational models:

Theorem 2. *Let $p \geq 2$, Γ_0 be a measurable subset of ∂D of positive measure, and let $\phi_0 : \Gamma_0 \to \mathbb{R}^3$ be a measurable function such that $\Phi = \{v \in W^{1,2p}(D),\, v = \phi_0$ on Γ_0, $\det \nabla v \in L^2(D)$, $\det \nabla v > 0$ a. e. on $D\}$ is not empty. Let $f \in L^\rho(D)$ and $g \in L^\sigma(\partial D \setminus \Gamma_0)$ be such that the linear form*

$$L : v \in W^{1,p}(D) \mapsto L(v) := \int_D f(x) \cdot v(x) dx + \int_{\partial D \setminus \Gamma_0} g(x) \cdot v(x) da(x)$$

is continuous (da denotes the surface measure), let

$$F(v) := \int_D W^p(\nabla v(x)) dx - L(v),$$

where W^p is either W^p_{T}, W^p_{AB}, or W^p_{V}, and assume that $\inf_{v\in\Phi} F(v) < \infty$. Then there exists at least one function $u \in \Phi$ such that

$$F(u) \,=\, \inf_{v\in\Phi} F(v).$$

Proof. We first treat the case of W^p_{T} and W^p_{AB} using polyconvexity, and then turn to W^p_{V} using results of [3].

Step 1. Proof for W^p_{T} and W^p_{AB}.
This is a direct application of Ball's seminal results of [6]. Since $2p \geq 3$, for all $v \in W^{1,2p}(D)$, $\det \nabla v \in L^1(D)$, and the set $\tilde{\Phi} := \{v \in W^{1,2p}(D), \det \nabla v \in L^2(D)\}$ is weakly-closed (see for instance [9, Section 7.6]). By Lemma 2, F is coercive on Φ and lower-semicontinuous for the weak-convergence in $\tilde{\Phi}$ (see [9, Section 7.7]). Let $u_n \in \Phi$ be a minimizing sequence of F on Φ. Up to extraction, u_n weakly converges to some $u \in \tilde{\Phi}$, and

$$F(u) \,\leq\, \inf_{v\in\Phi} F(v).$$

It remains to prove that $u \in \Phi$, which is a consequence of the property

$$\lim_{\det \xi \to 0} W^p(\xi) = +\infty,$$

and of the compactness of the trace operator, see for instance in [9, Section 7.7] for both arguments.

Step 2. Proof for W^p_{V}.
The structure of the proof is the same as above, noting that the lower-semicontinuity of F for the weak convergence in $W^{1,p}(D)$ is a direct consequence of Γ-convergence. We refer the reader to [3, Theorem 11] for details. □

5. Numerical approximation of the variational model

5.1. **The numerical solution method.** Our aim is to approximate $\xi \mapsto W_{\mathrm{V}}(\xi)$ with the help of (a variant of) formula (18):

$$W_{\mathrm{V}}(\xi) \,=\, \lim_{R\to\infty} \frac{1}{|B(R)|} \inf\{F_1(u, B_R), u \in \mathcal{S}(\mathcal{T}), u(x) = \xi \cdot x \text{ if } \mathrm{dist}(x, \partial B_R) \leq 2\mathbf{r}\}, \quad (21)$$

with W_{nn} given by (19), $W_{\mathrm{vol}} = W_{\mathrm{Helm}}$, and where $B(R)$ is the ball of radius $R > 0$ centered at the origin. Note that for the numerical approximation procedure we directly

consider $W_{\rm vol} = W_{\rm Helm}$, and do not use further regularization as in [2, Theorem 11] — this owes to the fact that this is the case of interest although we are not able to directly deal with $W_{\rm vol} = W_{\rm Helm}$ in the analysis yet. For the numerical approximation procedure one has to pick a large — though finite — $R \gg 1$, and minimize $F_1(\cdot, B_R)$ on the set of continuous and piecewise constant functions on $\mathcal{T} \cap B_R$ whose values on the boundary coincide with the affine deformation $x \mapsto \xi \cdot x$. To this aim, one needs to know $\mathcal{T} \cap B_R$. Yet, $\mathcal{T}$ is a Delaunay tessellation associated with a point process in the whole space $\mathbb{R}^3$. We therefore need to approximate the point process itself on the domain B_R. The point process we consider on $\mathbb{R}^3$ is the thermodynamic limit of the random parking measure associated with unit balls (that we will refer to as the "parking lattice"), which is rigorously defined as the limit of point processes on finite domains in [25]. As shown in [20], the parking lattice is stationary, ergodic, isotropic, almost surely general (the associated Delaunay tessellation is unique), and satisfies the hardcore and non-empty space conditions required by Theorem 1. Hence, formula (21) makes sense. The approximation of the parking lattice on finite domains B_R is as follows. For all $R > 0$, we make a uniform mesh of the sphere S_R of radius R (with triangles of side ~ 1) and consider a hardcore Poisson point process (with minimal distance 1) in B_{R-1} up to the packing limit (that is, until one cannot add any other point: due to the hardcore constraint, there is an easy upper bound on the number of points which can be accepted). In particular, for such a point process, any two points are at least at distance 1, and any ball of radius 1 has at least one point. We denote by $\mathcal{T}_R$ a Delaunay tessellation associated with the mesh of S_R and the points in B_{R-1}. As proved in [20], although $\mathcal{T}_R$ does not coincide with $\mathcal{T} \cap B_R$, we still have

$$\lim_{R\to\infty} \frac{1}{|B(R)|} \inf\{F_1(u, B_R), u \in \mathcal{S}(\mathcal{T}_R), u(x) = \xi \cdot x \text{ if } \mathrm{dist}(x, \partial B_R) \le 2\mathbf{r}\} \,=\, W_{\rm V}(\xi). \quad (22)$$

This is the final variant of (18) we consider, and which has the advantage to be *practically computable*.

The numerical approximation of (22) is made in two steps:

- We first generate the deterministic set of points on ∂B_R and a realization of the stochastic set of points in B_{R-1}. The latter is generated iteratively. Points are randomly picked in B_{R-1}. The first point is accepted. When another point is picked, either it is at distance less than 1 from a point which has already been accepted and it is discarded, or it is at distance at least 1 from all the other points and it is accepted. The algorithm stops when B_{R-1} is packed, that is, when no additional point can be accepted. Given the deterministic set of points on ∂B_R and the realization of the random set of points in B_{R-1} we then construct an associated Delaunay tessellation of B_R.
- In a second step, we solve the minimization problem associated with (22) for R finite and the Delaunay tessellation of B_R (well-defined as the minimization of a smooth coercive function on a finite-dimensional space) by a Newton algorithm, as it is classical in nonlinear elasticity (see for instance [22], and [29]) provided the addition of the energy of the edges (which are "non-standard" one-dimensional elements). Continuation methods are also used to ensure the convergence of the Newton algorithm.

In practice, we also consider several independent realizations of the stochastic set of point and make an empirical average of the approximations of $W_{\rm V}$ obtained. This enhances the convergence with respect to the randomness. For the analysis of numerical methods to approximate homogenized coefficients for random discrete systems, we refer the reader to the linear case dealt with in [16], based on [18, 19].

N_R	130	1600	6000	16000	33000	59500
K_R	2160	270	80	34	18	10

TABLE 1. Number of edges and associated number of realizations in the numerical computations.

Note that with respect to standard three-dimensional finite element methods, the solution of the minimization problem associated with (22) for R finite and the Delaunay tessellation of B_R requires to consider one-dimensional elements in addition to three-dimensional elements. These one-dimensional elements are represented by the edges of the tessellation.

At the end of the minimization algorithm, the homogenized energy $W_{\rm V}$ is approximated by the spatial average on B_R of the energy density of the minimizer which has been numerically obtained, and the Piola-Kirchhoff stress tensor is given by the spatial average on B_R of the associated local Piola-Kirchhoff stress tensor (provided the minimizer is isolated, and the local Hessian strongly elliptic, see [15, Section 4.2] for related arguments in the continuous case).

A study of the convergence of the numerical approximation of $W_{\rm V}(\xi)$ in terms of R and the number of realizations is proposed in the following paragraph for some typical values of ξ (both in small and large strains).

5.2. **Convergence properties.** In this subsection, we address some convergence properties related to the numerical approximation of $W_{\rm V}$. The numerical analysis of the numerical approximation procedure is made particularly difficult because

- the unknown is a vector and not a scalar,
- the system is nonlinear and nonconvex,
- the randomness is complex (the decorrelation properties of the random parking lattice are not easy to quantify).

As seen in [18, 19, 16] on a simpler linear scalar case, the error splits into two parts: a random error and a systematic error. The random error is of variance type and measures the fact that the computed quantities are random variables themselves. This error can be made as small as desired by using a sufficiently large number K_R of realizations. It is proved to decay at the central limit theorem scaling in terms of K_R times the number N_R of chains (in this scalar case, chains are viewed as conductances) in B_R in, that is $(K_R N_R)^{-1/2}$. The systematic error is related to the boundary conditions: we impose linear Dirichlet boundary conditions, which perturbs the energy — no matter the number of realizations. This error also vanishes at the limit $N_R \to \infty$. Its scaling is expected to be of the order R^{-1} since this is a surface effect — although there is no rigorous proof of this fact.

We have conducted two series of tests with two different strain gradients A_1 and A_2, the first in moderate deformation ($\sim 25\%$), and the second in large deformation ($\sim 300\%$):

$$A_1 = \begin{pmatrix} 1.1 & 0 & 0 \\ 0 & 1.2 & 0 \\ 0 & 0 & 25/33 \end{pmatrix}, \qquad A_2 = \begin{pmatrix} 2 & 0 & 0 \\ 0 & 3 & 0 \\ 0 & 0 & 1/6 \end{pmatrix}.$$

Both deformations are isochoric: $\det A_1 = \det A_2 = 1$.

We focus on the first Piola-Kirchhoff stress tensor $\frac{\partial W_{\rm V}(\xi)}{\partial \xi}$. We expect the stress tensors $\Pi_1(N_R, K_R) = [\Pi_1(N_R, K_R)]_{ij}$ and $\Pi_2(N_R, K_R) = [\Pi_2(N_R, K_R)]_{ij}$, associated with A_1 and A_2 respectiveley, to be diagonal. We therefore focus on the principal stresses. Each effective stress tensor is obtained as the empirical average over K_R realizations of a stochastic network in B_R (with approximately N_R edges). These numbers are gathered in Table 1.

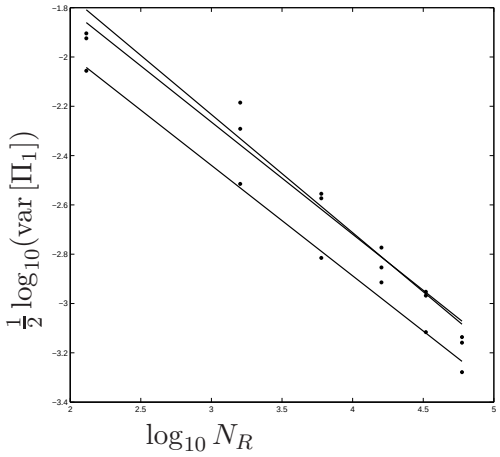

FIGURE 2. Variance of the diagonal terms of the Piola stress tensor for A_1 (range $[2,5]\times[-3.4,-1.8]$)

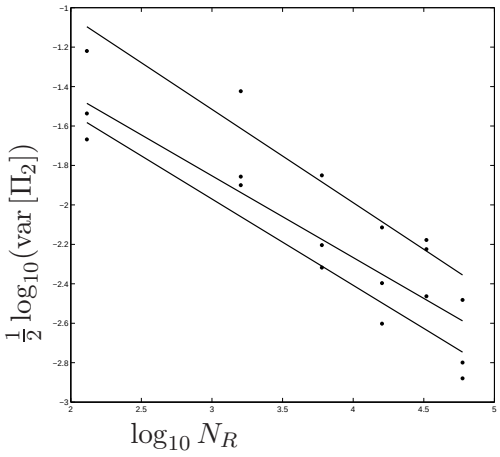

FIGURE 3. Variance of the diagonal terms of the Piola stress tensor for A_2 (range $[2,5]\times[-3,-1]$)

Id	0.4398	0.4775	0.3131
$\mathcal{R}_1$	0.4401	0.4790	0.3119
$\mathcal{R}_2$	0.4416	0.4772	0.3121
$\mathcal{R}_3$	0.4405	0.4786	0.3119

TABLE 2. Diagonal entries for the rotations of A_1

Id	0.8201	1.193	0.3246
$\mathcal{R}_1$	0.8209	1.197	0.3257
$\mathcal{R}_2$	0.8233	1.192	0.3256
$\mathcal{R}_3$	0.8215	1.192	0.3259

TABLE 3. Diagonal entries for the rotations of A_2

The (square root of the) variance of one realization is plotted for the three diagonal terms in function of N_R on Figure 2 for A_1 and Figure 3 for A_2, in log-log scale. The straight lines are linear fittings. Their slopes are approximately $-1/2$ (between $-.45$ and $-.5$), as expected.

To conclude, we show on Figures 4–6 and 7–9 the convergences of the diagonal terms of the Piola stress tensor (with the variance) in function of N_R, for A_1 and A_2, respectively. As can be seen, the systematic error error may largely dominate the random error (see in particular Figure 9). From now on, we shall consider that the approximation has converged for $N_R \sim 100000$ and $K_R \sim 10$.

5.3. **Isotropy of W_{V}.** The isotropy of the model is directly related to the isotropy of the network. To check the isotropy, we consider the two strain gradients A_1 and A_2 that we transform by the following three rotations:

$$\mathcal{R}_1 = \begin{pmatrix} 0 & 0 & 1 \\ 1 & 0 & 0 \\ 0 & 1 & 0 \end{pmatrix}, \mathcal{R}_2 = \begin{pmatrix} 0 & 1 & 0 \\ 0 & 0 & 1 \\ 1 & 0 & 0 \end{pmatrix}, \mathcal{R}_3 = \begin{pmatrix} 0 & 0 & 1 \\ \sqrt{2}/2 & -\sqrt{2}/2 & 0 \\ \sqrt{2}/2 & \sqrt{2}/2 & 0 \end{pmatrix}.$$

If W_{V} is isotropic, then the Piola stress tensor should transform as

$$\Pi(\mathcal{R}\xi) \;=\; \mathcal{R}\Pi(\xi).$$

For A_1 and A_2, and each of the three rotations, the diagonal entries of ${}^T\mathcal{R}_i\Pi(\mathcal{R}_i A_j)$ are reported on in Tables 2 and 3. The difference with $\Pi(A_j)$ is a measure of the anisotropy. As can be seen, the difference on the diagonal terms is of order 0.1%, which shows the network can be considered isotropic, and that the energy density W_{V} is indeed isotropic.

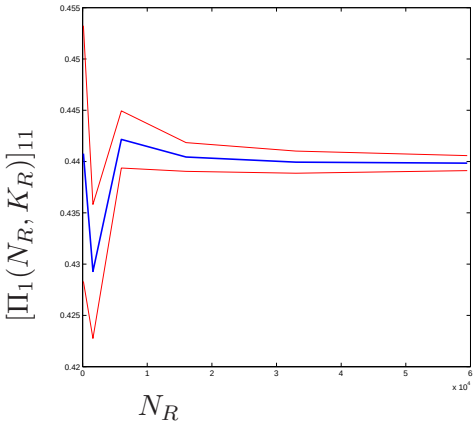

FIGURE 4. Convergence of the diagonal part 1 of the Piola stress tensor for A_1 (range $[0, 6\,10^4] \times [0.42, 0.46]$)

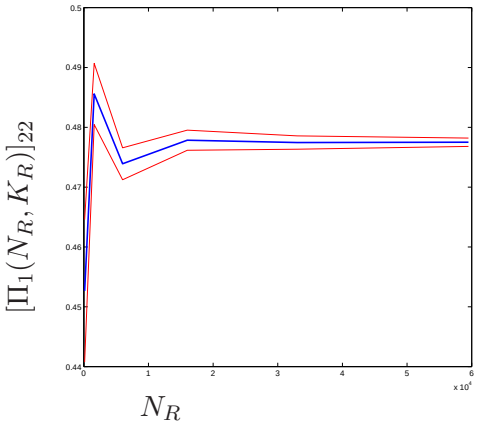

FIGURE 5. Convergence of the diagonal part 2 of the Piola stress tensor for A_1 (range $[0, 6\,10^4] \times [0.44, 0.5]$)

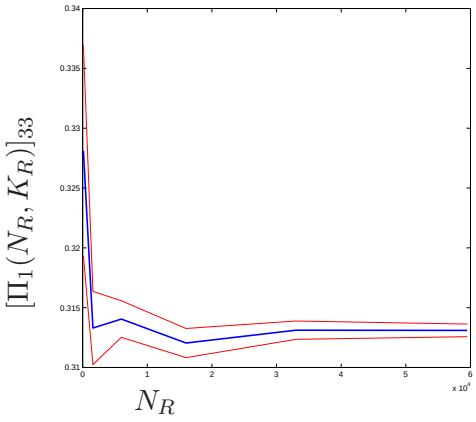

FIGURE 6. Convergence of the diagonal part 3 of the Piola stress tensor for A_1 (range $[0, 6\,10^4] \times [0.31, 0.34]$)

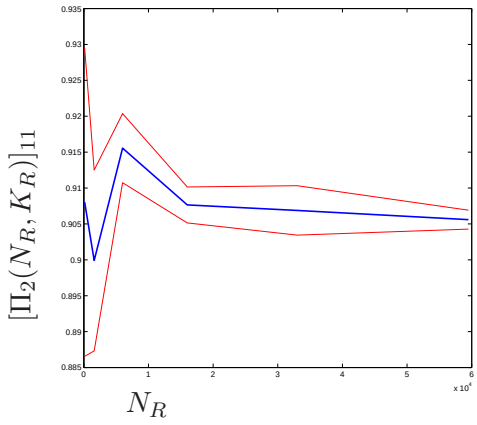

FIGURE 7. Convergence of the diagonal part 1 of the Piola stress tensor for A_2 (range $[0, 6\,10^4] \times [0.88, 0.94]$)

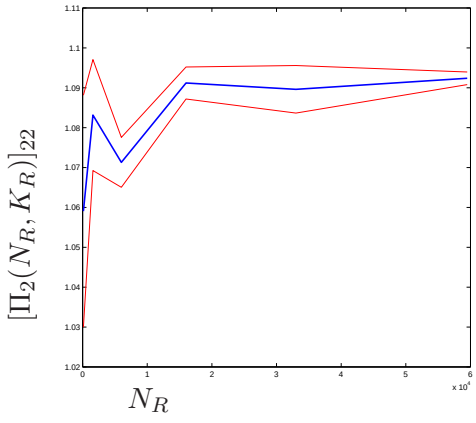

FIGURE 8. Convergence of the diagonal part 2 of the Piola stress tensor for A_2 (range $[0, 6\,10^4] \times [1.02, 1.11]$)

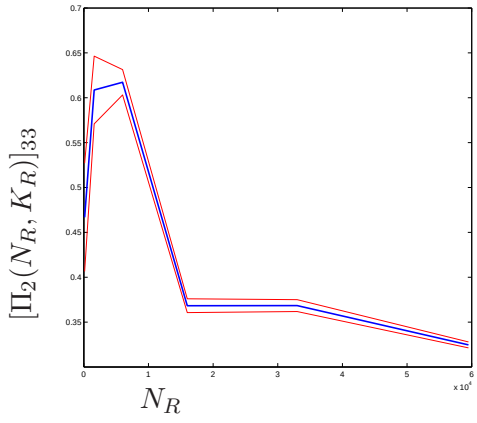

FIGURE 9. Convergence of the diagonal part 3 of the Piola stress tensor for A_2 (range $[0, 6\,10^4] \times [0, 0.7]$)

5.4. **Dependence on the second invariant.** It is rather well admitted that the energy density of rubber materials slightly depends on the second invariant I_2 of the Cauchy-Green strain tensor. By definition, the Arruda-Boyce model only depends on the first and third invariants. As would show a elementary series expansion, the Treloar model actually depends on the second invariant — although the coefficient in front of I_2 is actually rather small compared to the coefficient for I_1. This is also the case for the variational model as we shall show now. Without anticipating too much, note that Treloar's experiments do not allow to check the dependence with respect to I_2.

We write the energy as a function of the invariants I_1, I_2, and I_3, so that

$$W_V(\xi) \,=\, \omega(I_1, I_2, I_3)$$

for some function $\omega : \mathbb{R}^3_+ \to \mathbb{R}_+$. This implies for a deformation of the form $\xi = \mathrm{diag}(\xi_1, \xi_2, \xi_3)$ that the Piola stress tensor is diagonal, and that its entries are given for all $i \in \{1, 2, 3\}$ by

$$\Pi(\xi)_{ii} \,=\, 2\xi_i \frac{\partial \omega}{\partial I_1}(I_1, I_2, I_3) + 2\xi_i (I_1 - \xi_i^2) \frac{\partial \omega}{\partial I_2}(I_1, I_2, I_3) + \frac{2I_3}{\xi_i} \frac{\partial \omega}{\partial I_3}(I_1, I_2, I_3).$$

Let us fix some $i_1 > 0$ and $i_3 = 1$, and set $\alpha(I_2) = 2\frac{\partial \omega}{\partial I_1}(i_1, I_2, i_3)$, $\beta(I_2) = 2\frac{\partial \omega}{\partial I_2}(i_1, I_2, i_3)$, and $\gamma(I_2) = 2\frac{\partial \omega}{\partial I_3}(i_1, I_2, i_3)$. Then, for all $\xi = \mathrm{diag}(\xi_1, \xi_2, \xi_3)$ such that $I_1 = i_1$ and $I_3 = i_3$, the Piola stress tensor is given by

$$\Pi(\xi) \,=\, \alpha(I_2)\xi + \beta(I_2)\mathrm{diag}(\xi_1(i_1 - \xi_1^2), \xi_2(i_1 - \xi_2^2), \xi_3(i_1 - \xi_3^2)) + \gamma(I_2)\mathrm{diag}(\xi_1^{-1}, \xi_2^{-1}, \xi_3^{-1}). \tag{23}$$

In particular, W does not depend on I_2 if α and γ are constant functions, and if in addition $\beta \equiv 0$.

We have conducted numerical tests with $i_1 = 9$ and $i_3 = 1$ for the following three deformation gradients ξ:

$$\begin{aligned} \xi^1 &= \mathrm{diag}(1, 2.8058837, 0.35639401), \\ \xi^2 &= \mathrm{diag}(1.7320508, 2.4380156, 0.2368116), \\ \xi^3 &= \mathrm{diag}(2, 3.461088, 0.1444632). \end{aligned}$$

These deformation gradients ξ^1, ξ^2, ξ^3 satisfy $I_2 = 9, 18.333333, 48.25$, respectively. For each deformation gradient, we have computed α, β, and γ by solving a 3×3 linear system. Caution should be taken since the systematic and random error in the computations may be of the order of the coefficients β and γ. We have therefore made explicit a confidence interval, which corresponds to the variance of the coefficients for several realizations (of the polymer network). Tables 4 and 5 report on the values of α, β, and γ and of their variances for each deformation gradient (with 100 realizations), for the Treloar and the variational model, respectively. Note that the results on the Treloar model are obtained numerically using the same meshes as for the variational model and within the affine assumption, so that there is also statistical variability due to the randomness of the meshes.

The dependence of the Treloar model upon the second invariant is clear for ξ_1, ξ_2 and ξ_3 since the random error on β is of order of 10%. For the variational model, the order of magnitude of β and its sign seem reasonable. Yet, the error is of the order of 50% for the cases ξ_1 and ξ_2. For the case ξ_3, the error is only of the order of 10%, which clearly shows that the variational model also slightly depends on the second invariant.

5.5. **Validity of the affine assumption.** The affine assumption states that the deformation of the sample B_R which minimizes the energy for the Dirichlet boundary conditions $x \mapsto \xi \cdot x$ is close enough to the linear deformation $x \mapsto \xi \cdot x$ in B_R so that it can be replaced by the the linear deformation for the computation of $W_{\mathrm{V}}(\xi)$ through (22), and

	α	$\Delta\alpha$	β	$\Delta\beta$	γ	$\Delta\gamma$
ξ^1	0.3151	$\pm$ 0.0015	- 0.00342	$\pm$ 0.00022	0.00012	$\pm$ 0.00017
ξ^2	0.3144	$\pm$ 0.0020	- 0.00334	$\pm$ 0.00041	0.000043	$\pm$ 0.00012
ξ^3	0.3290	$\pm$ 0.0015	- 0.00372	$\pm$ 0.00028	0.000040	$\pm$ 0.000037

TABLE 4. Set of parameters for the Treloar model

	α	$\Delta\alpha$	β	$\Delta\beta$	γ	$\Delta\gamma$
ξ^1	0.2898	$\pm$ 0.00075	- 0.00040	$\pm$ 0.00017	0.02177	$\pm$ 0.00032
ξ^2	0.2888	$\pm$ 0.0015	- 0.00057	$\pm$ 0.00034	0.01833	$\pm$ 0.00021
ξ^3	0.3063	$\pm$ 0.00040	- 0.00131	$\pm$ 0.00013	0.042400	$\pm$ 0.00058

TABLE 5. Set of parameters for the variational model

of $\Pi(\xi)$ (the associated Piola stress tensor). In what follows, we denote by $\tilde{\Pi}(\xi)$ the Piola stress tensor computed with the linear deformation (that is, within the affine assumption).

Our numerical experiments show there are two distinct regimes: at moderate deformation, the affine assumption seems to be justified, whereas at large deformation, nonlinear effects play an important role. The threshold above which nonlinear effects are important depends on two parameters:

- the relative strength K of the volumetric term $W_{\rm Helm}$ (the higher, the closer to the affine assumption),
- the connectivity of the network (the higher, the more rigid).

To illustrate this, we have gathered in Figure 10 numerical simulations in uniaxial traction within the affine assumption (the Treloar model), and for the variational model with three different constants for the Helmholtz energy: $K = 5, 50, 500$. More precisely, the deformation gradient ξ is of the form

$$\xi = \mathrm{diag}(\lambda, \lambda^{-1/2}, \lambda^{-1/2})$$

for some $\lambda \geq 1$, and we have plotted the so-called the so-called engineering stress given by

$$S_{\rm uniaxial} = \frac{\sigma_{11} - \sigma_{22}}{\lambda}.$$

As announced, the constant K controls the threshold of non-affinity. On Figure 11, we have plotted the numerical simulations for Treloar's data in extension for two different networks: the original network obtained from the parking lattice (connectivity around 20), and a modification of this network where edges have been randomly deleted to obtain a connectivity around 4. Both the affine and variational models are represented for $K = 50$, and support the fact that connectivity controls the threshold of non-affinity as well.

Let us conclude this discussion by looking more closely at this nonlinear effect. We turn to the two matrices A_1 and A_2 considered in Section 5. For $N_R = 59500$, $K_R = 10$, and $K = 100$, the first Piola stress tensors are denoted by $\tilde{\Pi}$ for the Treloar model, and by Π for the variational model. They are given by for A_1 by

$$\begin{aligned} \Pi_1(N_R, K_R) &= \mathrm{diag}(0.430, 0.478, 0.313), \\ \tilde{\Pi}_1(N_R, K_R) &= \mathrm{diag}(0.443, 0.484, 0.306), \end{aligned}$$

and for A_2 by

$$\begin{aligned} \Pi_2(N_R, K_R) &= \mathrm{diag}(0.820, 1.19, \mathbf{0.324}), \\ \tilde{\Pi}_2(N_R, K_R) &= \mathrm{diag}(0.824, 1.25, \mathbf{0.0681}). \end{aligned}$$

For A_1, the difference on the diagonal terms is quite small, 0.7%, 1%, and 2%, respectively. This is completely negligible in comparison to the convergence error in N_R. Yet, for A_2,

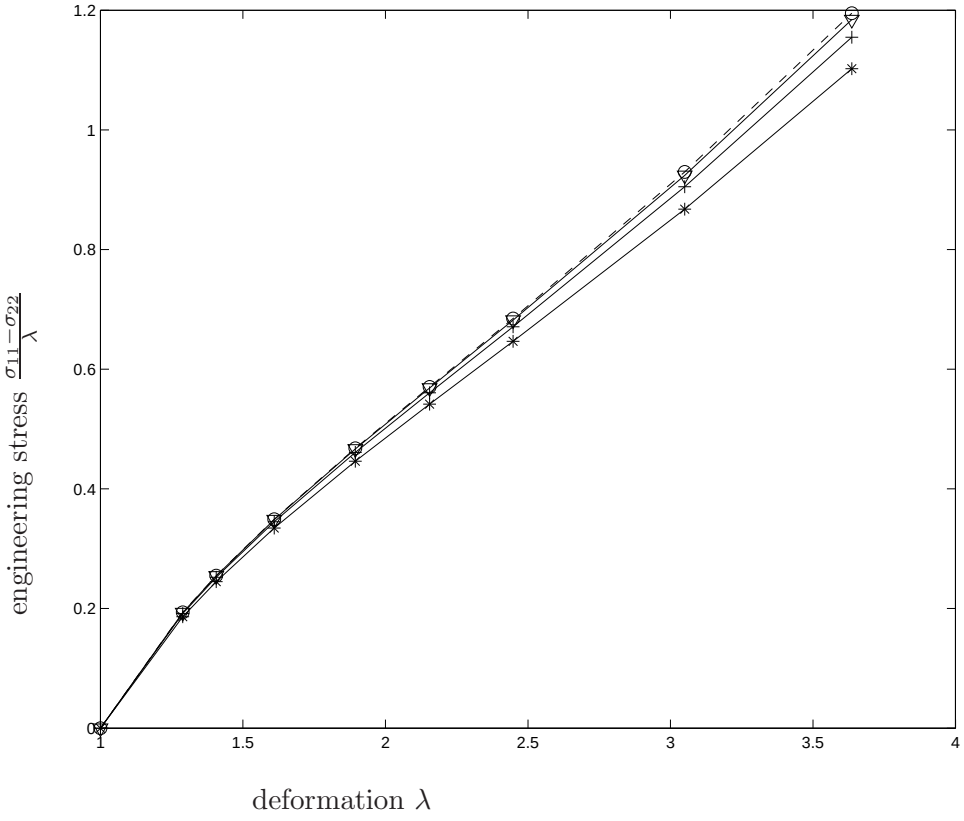

FIGURE 10. Uniaxial traction — affine assumption (dashed line), variational model for $K = 500, 50, 5$ and connectivity 20 (from top to bottom)

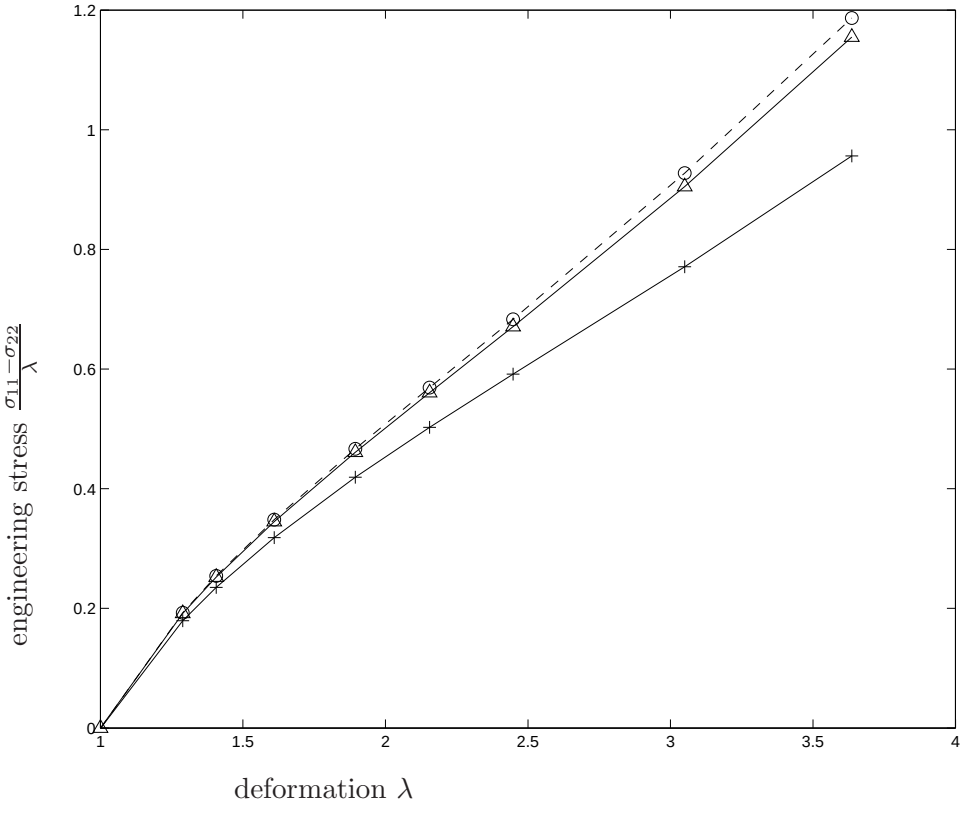

FIGURE 11. Uniaxial traction — affine assumption (dashed line), variational model for $K = 50$ and connectivities 20 and 4 (from top to bottom)

the difference on the diagonal terms can be quite important and cannot be neglected: 0.4%, 5%, and 79%, respectively.

In this subsection we have put in evidence the interplay between non-affinity, the connectivity of the network, and the volumetric term in the energy. Physics should in principle guide us for the connectivity of the network and the volumetric term (recall Remark 2). Note that this interplay is beyond the scope of both the Treloar model (since this is a nonlinear effect due to the non-affinity) and the Arruda-Boyce model (since the network is reduced there to eight chains — there is no connectivity at all).

5.6. **The Rivlin effect.** In the experiment literature, models are usually compared using the so-called Mooney plot, which is sensitive to relative errors. For uniaxial experiments, whose deformation imposed at the boundary is typically given by the linear map

$$\xi = \mathrm{diag}(\lambda, \lambda^{-1/2}, \lambda^{-1/2})$$

for $\lambda > 0$, the Mooney plot consists in dividing the engineering stress

$$S_{\mathrm{uniaxial}} = \frac{\sigma_{11} - \sigma_{22}}{\lambda}$$

by the universal geometrical factor $2(\lambda - 1/\lambda^2)$, plotted against $1/\lambda$. In particular, a material exhibits the so-called Rivlin effect if the curve of the Mooney stress

$$\frac{1}{\lambda} \mapsto \frac{\sigma_{11}(\lambda) - \sigma_{22}(\lambda)}{2(\lambda^2 - 1/\lambda)}$$

is strictly concave around $\lambda = 1$. Rubber materials generically exhibit such a Rivlin effect, see for instance Figure 9 in [26].

It is therefore of interest to check whether this is the case as well for the discrete variational model for rubber introduced in this article (note that the Arruda-Boyce model cannot exhibit a Rivlin effect).

Numerical tests show that the concavity of this curve is driven by the average number of monomers N per polymer chain. For small number of monomers (typically $N = 25$), there is no Rivlin effect, and the curve is flat around $\lambda = 1$. For larger number of monomers (typically $N = 250$), there is a significant Rivlin effect, and the curve is strictly concave around $\lambda = 1$. This dependence upon N is due to the form of the inverse Langevin function, which somehow forbids relaxation for small N. Figure 13 illustrates the numerical Rivlin effect for $N = 250$ and $A = 5$ in logarithmic scale for $1/\lambda$, whereas Figure 12 illustrates the (almost) absence of Rivlin effect for $N = 25$ and $A = 5$. Note that the closer to $\lambda = 1$ the less reliable the points (since the denominator is singular at $\lambda = 1$). Yet, for $\lambda = 1$ one may approximate the Mooney stress by using a Taylor expansion of both the numerator and the denominator (this requires the knowledge of the second derivative of the energy, which is an output of the numerical method used to approximate the variational model). The point at $\lambda = 1$ is therefore reliable, and the curve is clearly strictly concave around $\lambda = 1$ for $N = 250$, as expected of rubber materials.

6. Comparison of the three models

6.1. **General relations for the energy.** The energy densities satisfy the following general relations

$$\left.\begin{array}{l} W_{\mathrm{V}}(\xi) \\ W_{\mathrm{AB}}(\xi) \end{array}\right\} \leq W_{\mathrm{T}}(\xi). \tag{24}$$

The first inequality holds because the linear deformation is a test function for the minimization problem defining W_{V} whereas the second inequality is a consequence of Jensen's

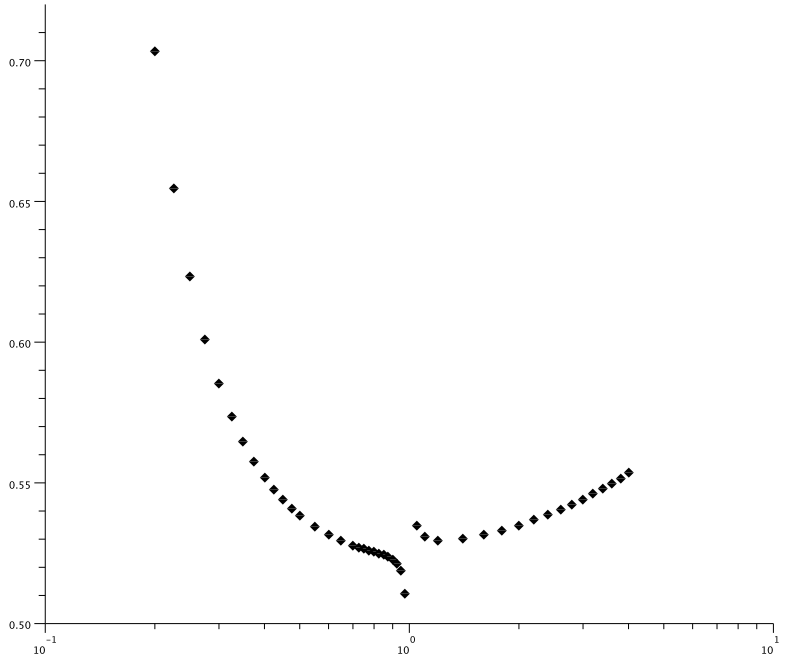

FIGURE 12. Mooney plot $1/\lambda \mapsto \frac{\sigma_{11}-\sigma_{22}}{2(\lambda^2-1/\lambda)}$ in the case of small chains (N=25). The curve is locally flat, indicating that there is no Rivlin effect.

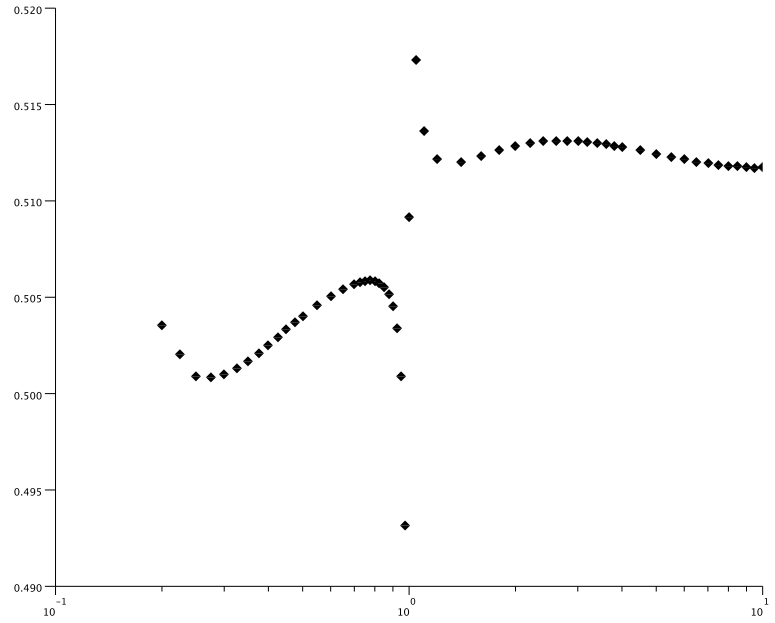

FIGURE 13. Mooney plot $1/\lambda \mapsto \frac{\sigma_{11}-\sigma_{22}}{2(\lambda^2-1/\lambda)}$ in the case of long chains (N=250). The curve is locally concave, indicating that there is a distinct Rivlin effect in the variational model

inequality:

$$\begin{aligned}
\tilde{W}^p_{\mathrm{T}}(\xi) &= \frac{1}{4\pi}\int_0^{\pi}\int_0^{2\pi} W_c^p(\lambda_1^2\cos^2\phi+\lambda_2^2\sin^2\phi\cos^2\theta+\lambda_3^2\sin^2\phi\sin^2\theta)\sin\phi d\theta d\phi \\
&= \frac{1}{4\pi}\int_{-1}^{1}\int_0^{2\pi} W_c^p(\lambda_1^2 s^2+\lambda_2^2(1-s^2)\cos^2\theta+\lambda_3^2(1-s^2)\sin^2\theta)d\theta ds \\
&\geq W_c^p\left(\frac{1}{4\pi}\int_{-1}^{1}\int_0^{2\pi}(\lambda_1^2 s^2+\lambda_2^2(1-s^2)\cos^2\theta+\lambda_3^2(1-s^2)\sin^2\theta)d\theta ds\right) \\
&= W_c^p\left(\frac{\lambda_1^2+\lambda_2^2+\lambda_3^2}{3}\right) \\
&= \tilde{W}^p_{\mathrm{AB}}(\xi),
\end{aligned}$$

where W_c^p is such that for N fixed, $W_c^p(r^2/(Nl^2)) = \tilde{W}_c(r,N)$ for all $r \geq 0$.

Although these general relations only hold for the energy density, this suggests that the Arruda-Boyce and variational models are softer than the Treloar model. We thus expect principal stresses to be higher for the Treloar model. This is actually what we observe in the following subsection.

6.2. **Comparison to Treloar's experiments.** In this subsection we compare the three models to Treloar's experiments. The plots 14, 15, and 16 display the engineering stresses (or nominal stresses) associated with the mechanical experiments in uniaxial traction, biaxial traction, and in planar tension, respectively. Let us quickly recall the definitions of the engineering stress for these three types of sollicitation. Uniaxial traction corresponds to a deformation gradient ξ of the form

$$\xi = \mathrm{diag}(\lambda, \lambda^{-1/2}, \lambda^{-1/2})$$

for some $\lambda \geq 1$. The quantity $\lambda - 1$ is called the engineering strain. The associated Cauchy stress tensor σ is diagonal, and the associated engineering stress is given by

$$\lambda - 1 \mapsto S_{\mathrm{uniaxial}} = \frac{\sigma_{11}-\sigma_{22}}{\lambda}.$$

For biaxial traction the deformation gradient ξ is of the form

$$\xi = \mathrm{diag}(\lambda^{-2}, \lambda, \lambda)$$

for some $\lambda \geq 1$. The quantity $\lambda^{-2} - 1$ is called the engineering strain. The associated Cauchy stress tensor σ is diagonal, and the associated engineering stress is given by

$$\lambda^{-2} - 1 \mapsto S_{\mathrm{biaxial}} = \frac{\sigma_{11}-\sigma_{22}}{\lambda^{-2}}.$$

Finally, the planar tension experiment corresponds to a deformation gradient ξ of the form

$$\xi = \mathrm{diag}(1, \lambda, \lambda^{-1})$$

for some $\lambda \geq 1$. The quantity $\lambda - 1$ is called the engineering strain. The associated Cauchy stress tensor σ is diagonal, and the associated engineering stress is given by

$$\lambda - 1 \mapsto S_{\mathrm{planar}} = \frac{\sigma_{22}-\sigma_{11}}{\lambda}.$$

For the Arruda-Boyce model, we have used standard coefficients to fit Treloar's data, namely $N = 26.5$ and $\frac{n}{\beta} = 0.27$. For the numerical simulation of the variational model, the stochastic network has been generated by the random parking lattice. We have not tried to optimize the parameters further, and have taken $N = 26.5$ and $\frac{n}{\beta} = 0.27$ as well, and set $K = 5$ (ultimately, this last parameter will have to be optimized together with the connectivity of the network, see Section 7).

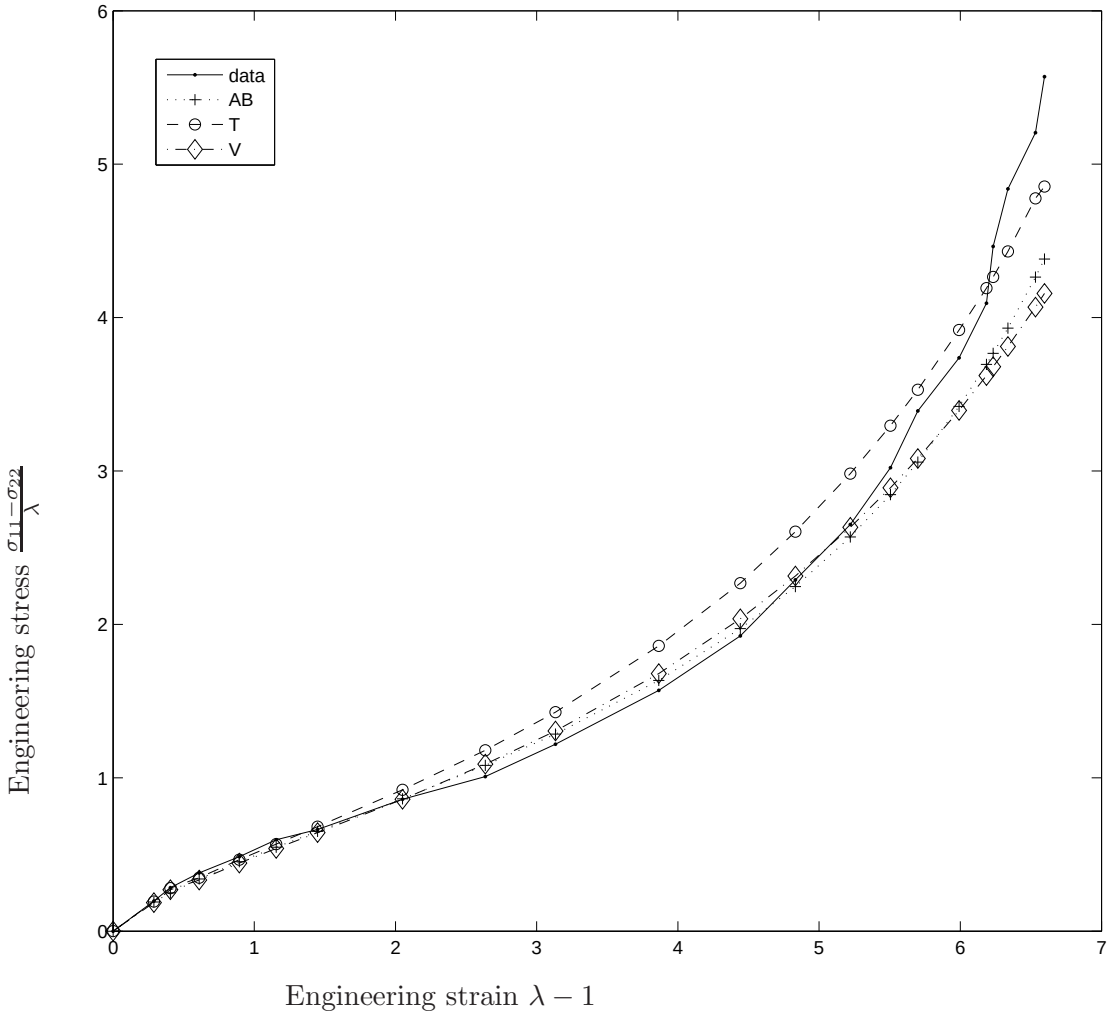

FIGURE 14. Uniaxial traction — Treloar's experiments

6.3. **Comparison of the Cauchy stress tensors for general deformations.** Although the comparison to Treloar's experiments seem to reveal that the Arruda-Boyce and the variational models are very close to each other, a closer look at the results shows there are significant differences. In particular, we have only compared the engineering stress, and not the full Cauchy stress tensor (which is unavailable in Treloar's experiments). Let us go back to the case of uniaxial extension. For moderate deformation, the three models yield similar engineering stress. The same conclusion holds for the Cauchy stress tensor. We first consider the following strain gradient

$$A = \mathrm{diag}(1.8945,\, 0.7265286,\, 0.7265286),$$

the three Cauchy stress tensors are given by:

$$\begin{aligned} \Sigma_{\mathrm{T}} &= \mathrm{diag}(1.03,\, 0.147,\, 0.147), \\ \Sigma_{\mathrm{V}} &= \mathrm{diag}(1.00,\, 0.154,\, 0.154), \\ \Sigma_{\mathrm{AB}} &= \mathrm{diag}(1.01,\, 0.148,\, 0.148). \end{aligned}$$

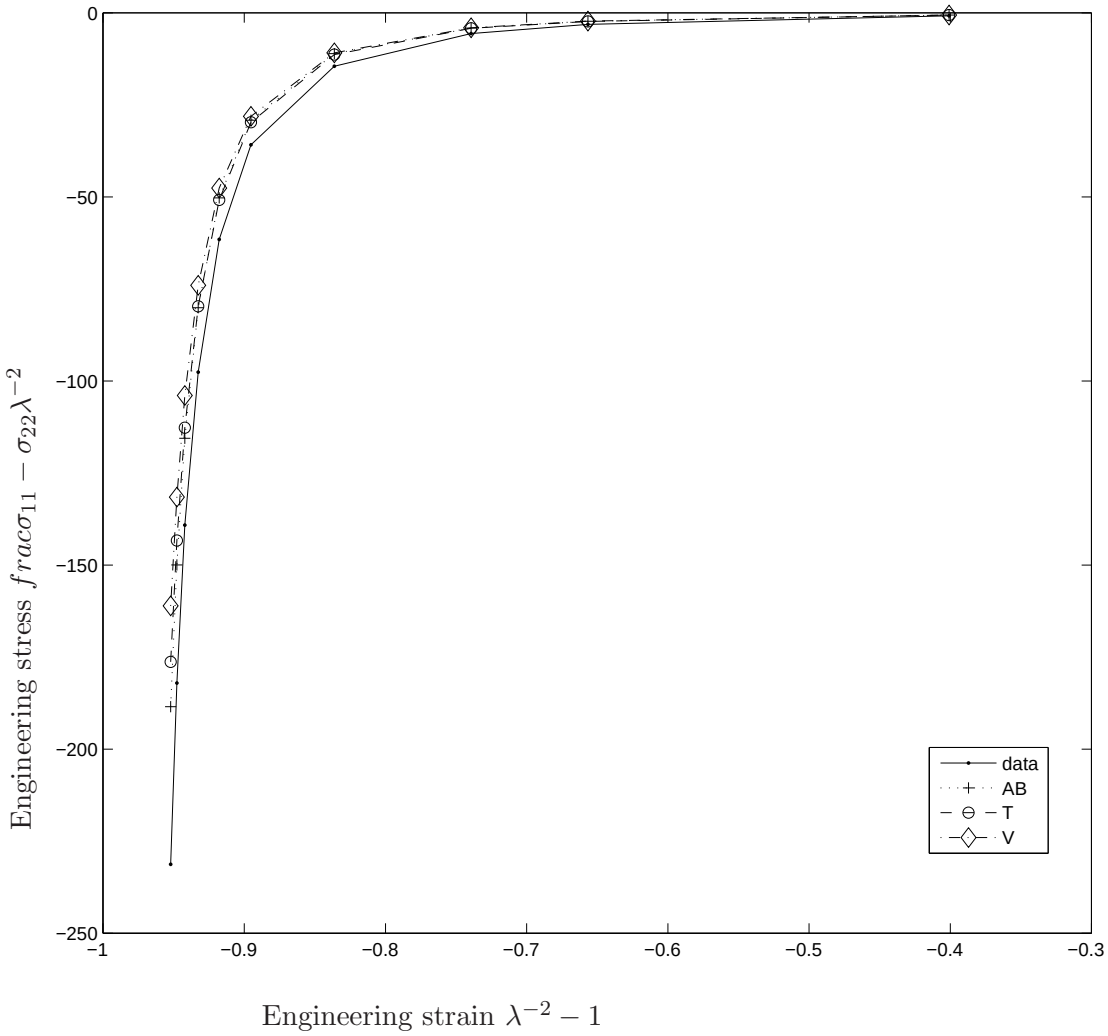

FIGURE 15. Biaxial tension — Treloar's experiments

As can already be seen, the counterpart to decrease the uniaxial stress is to increase the transversal stresses. This tendency seems to be more pronounced for the variational model. This is even clearer in larger deformation. For the strain gradient

$$A = \mathrm{diag}(6.5052,\ 0.3920755,\ 0.3920755)$$

the three Cauchy stress tensors are given by:

$$\begin{aligned} \Sigma_{\mathrm{T}} &= \mathrm{diag}(21.5,\ 0.0523,\ 0.0525), \\ \Sigma_{\mathrm{V}} &= \mathrm{diag}(18.9,\ 0.146,\ 0.146), \\ \Sigma_{\mathrm{AB}} &= \mathrm{diag}(18.6,\ 0.0675,\ 0.0675). \end{aligned}$$

In order to decrease the uniaxial stress the variational model increases a lot the normal stresses, whereas the Arruda-Boyce model is much less sensitive to this effect.

Using the two matrices A_1, and A_2, we have for the three Cauchy stress tensors:

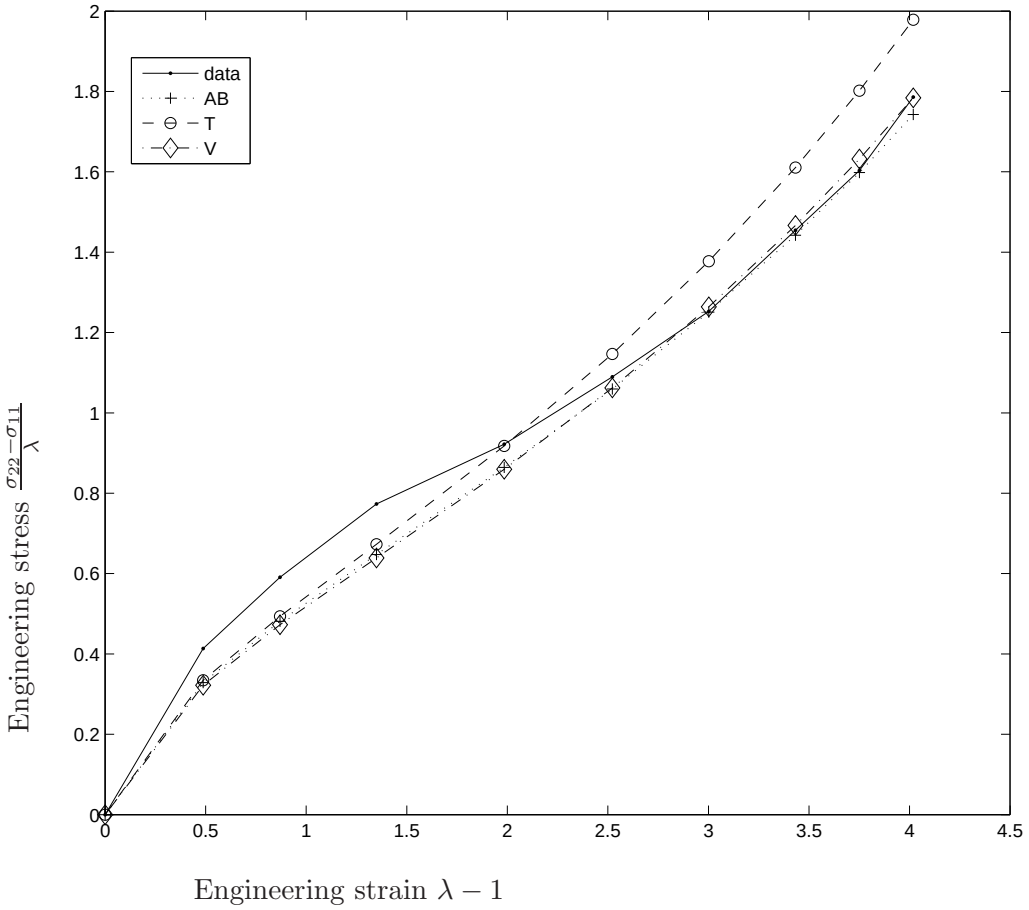

FIGURE 16. Planar tension— Treloar's experiments

$$\begin{aligned} \Sigma^1_{\mathrm{T}} &= \mathrm{diag}(0.48,\, 0.58,\, 0.23) & \Sigma^2_{\mathrm{T}} &= \mathrm{diag}(1.6,\, 3.8,\, 0.011) \\ \Sigma^1_{\mathrm{V}} &= \mathrm{diag}(0.48,\, 0.57,\, 0.24) & \Sigma^2_{\mathrm{V}} &= \mathrm{diag}(1.6,\, 3.6,\, 0.054) \\ \Sigma^1_{\mathrm{AB}} &= \mathrm{diag}(0.33,\, 0.40,\, 0.16) & \Sigma^2_{\mathrm{AB}} &= \mathrm{diag}(1.2,\, 2.7,\, 0.0084). \end{aligned}$$

In these cases, the Cauchy stress tensors are very different, and the Arruda-Boyce model relaxes much more the stress.

Note that the conclusions strongly depend on the strength K of the volumetric energy density and on the connectivity of the network regarding the variational model.

7. PERSPECTIVES

In this article we have presented three discrete models for rubber: the Treloar model, the Arruda-Boyce model, and a variational model based on the statistical physics of reticulated polymer chains. In particular we have seen that the three models yield nice mathematical and mechanical properties, and compared them to Treloar's experiments. The comparison of the variational model to Treloar's experiments is promising, and there is room for improvement of the model using more physical input (essentially more information on the polymer-chain network). The following program should be addressed to go further:

- generate more realistic networks in terms of connectivity and molecular mass (we expect a better relaxation at moderate strain and still an increase of the stiffness at large strain);

- find explicit formulas for the constitutive law W_V by solving an inverse problem in order to turn the model into an attractive alternative to the engineering community;
- compare the simulations to physical experiments at the scale of the polymer-chain network (this would challenge the validity of the discrete model itself).

These three issues will be addressed in future works.

Acknowledgments

We gratefully acknowledge the help of Eric Saltel and Paul-Louis Georges from the project-team GAMMA of INRIA for providing us with a customized Delaunay tessellation software, and the stimulating discussions on the subject with François Lequeux and Michael Rubinstein. The research of the authors was supported by INRIA, under the grant "Action de Recherche Collaborative" DISCO.

References

[1] R. Alicandro, M. Cicalese, and A. Gloria. Mathematical derivation of a rubber-like stored energy functional. *C. R. Acad. Sci. Paris, Série I*, 345(8):479–482, 2007.

[2] R. Alicandro, M. Cicalese, and A. Gloria. Convergence analysis of the Böl-Reese discrete model for rubber. In *Proceedings of the 11th International Symposium on Continuum Models and Discrete Systems*, 2008.

[3] R. Alicandro, M. Cicalese, and A. Gloria. Integral representation results for energies defined on stochastic lattices and application to nonlinear elasticity. *Arch. Ration. Mech. Anal.*, 200(3):881–943, 2011.

[4] E.M. Arruda and M.C. Boyce. A three-dimensional constitutive model for the large stretch behavior of rubber elastic materials. *Journal of the Mechanics and Physics of Solids*, 41:389–412, 1993.

[5] E.M. Arruda and M.C. Boyce. Constitutive models of rubber elasticity : a review. *Rubber Chemistry and Technology*, 72:504–523, 2000.

[6] J.M. Ball. Convexity conditions and existence theorems in nonlinear elasticity. *Arch. Rat. Mech. Anal.*, 63:337–403, 1977.

[7] M. Böl and S. Reese. Finite element modelling of rubber-like materials - a comparison between simulation and experiment. *Journal of Materials Sc.*, 40:5933–5939, 2005.

[8] M. Böl and S. Reese. Finite element modelling of rubber-like polymers based on chain statistics. *Int. J. Sol. Struc.*, 43:2–26, 2006.

[9] P.G. Ciarlet. *Mathematical elasticity. Volume I: three-dimensional elasticity*, volume 20 of *Studies in Mathematics and its Applications*. North-Holland Publishing Co., Amsterdam, 1988.

[10] M. De Buhan, A. Gloria, P. Le Tallec, and M. Vidrascu. Reconstruction of a constitutive law for rubber from in silico experiments. In preparation.

[11] B. N. Delone, N. P. Dolbilin, M. I. Štogrin, and R. V. Galiulin. A local test for the regularity of a system of points. *Dokl. Akad. Nauk SSSR*, 227(1):19–21, 1976.

[12] P.J. Flory. *Statistical mechanics of chain molecules*. Interscience Publishers, New York, 1969.

[13] G. Geymonat, S. Müller, and N. Triantafyllidis. Homogenization of nonlinearly elastic materials, microscopic bifurcation and macroscopic loss of rank-one convexity. *Arch. Rat. Mech. Anal.*, 122:231–290, 1993.

[14] A. Gloria. Strong ellipticity of nonlinear elastic materials and homogenization of periodic and stochastic discrete systems. In preparation.

[15] A. Gloria. A direct approach to numerical homogenization in finite elasticity. *Netw. Heterog. Media.*, 1:109–141, 2006.

[16] A. Gloria. Numerical approximation of effective coefficients in stochastic homogenization of discrete elliptic equations. *M2AN Math. Model. Numer. Anal.*, 46(1):1–38, 2012.

[17] A. Gloria, P. Le Tallec, F. Lequeux, and M. Vidrascu. In preparation.

[18] A. Gloria and F. Otto. An optimal variance estimate in stochastic homogenization of discrete elliptic equations. *Ann. Probab.*, 39(3):779–856, 2011.

[19] A. Gloria and F. Otto. An optimal error estimate in stochastic homogenization of discrete elliptic equations. *Ann. Appl. Probab.*, 22(1):1–28, 2012.

[20] A. Gloria and M.D. Penrose. Random parking, Euclidean functionals, and rubber elasticity. 2012. Preprint.

[21] W. Kuhn and F. Grün. Beziehung zwischen elastische Konstanten und Dehnungsdoppelberechnung Eigenschaften hochpolymerer Stoffe. *Kolloid-Zeitschrift*, 101:248–271, 1942.

[22] P. Le Tallec. Numerical methods for nonlinear three-dimensional elasticity. In *Handbook of numerical analysis, Vol. III*, pages 465–622. North-Holland, 1994.
[23] P. Le Tallec. *Mécanique des Milieux Continus*. Editions de l'École polytechnique, 2006.
[24] V.J. Mizel. On the ubiquity of fracture in nonlinear elasticity. *J. Elasticity*, 52:257–266, 1999.
[25] M.D. Penrose. Random parking, sequential adsorption, and the jamming limit. *Commun. Math. Phys.*, 218:153–176, 2001.
[26] M. Rubinstein and S. Panyukov. Elasticity of polymer networks. *Macromolecules*, 35:6670–6686, 2002.
[27] D. Ruelle. *Statistical mechanics. Rigorous results*. World Scientific Publishing Co., Inc., River Edge, NJ; Imperial College Press, London, 1999. Reprint of the 1989 edition.
[28] L.R.G Treloar. *The Physics of Rubber Elasticity*. Oxford at the Clarendon Press, Oxford, 1949.
[29] M. Vidrascu. Solution of non-linear elasticity problems using the *continu* software. *Inria Report Research (http://www.inria.fr/rrrt/rr-4128.html)*, 2001.